Drainage evolution and exhumation history of the eastern Himalaya: Insights from the Nicobar Fan, northeastern Indian Ocean

Wen-Huang Chen[1, 2, 3*], Yi Yan[1*], Peter D. Clift[4], Andrew Carter[5], Chi-Yue Huang[6], Kevin T. Pickering[7], Farid Chemale Jr.[8], Yehua Shan[1], and Xinchang Zhang[1]

[1]Key Laboratory of Ocean and Marginal Sea Geology, Guangzhou Institute of Geochemistry, Chinese Academy of Sciences, Guangzhou 510640, China

[2]Southern Marine Science and Engineering Guangdong Laboratory (Guangzhou), Guangzhou 511458, China

[3]Innovation Academy of South China Sea Ecology and Environmental Engineering, Chinese Academy of Sciences, Guangzhou, 510640, China

[4]Department of Geology and Geophysics, Louisiana State University, Baton Rouge, LA 70803, USA

[5]Department of Earth and Planetary Sciences, Birkbeck, University of London, Malet Street, London WC1E 7HX, United Kingdom

[6]School of Ocean and Earth Science, Tongji University, Shanghai 200092, China

[7]Department of Earth Sciences, University College London (UCL), London WC1E 6BT, United Kingdom

[8]Programa de Pós-Graduação em Geologia, Universidade do Vale do Rio dos Sinos, 93.022-750 São Leopoldo, RS, Brazil

*Corresponding Authors: Wen-Huang Chen, chenwenhuang@gig.ac.cn, and Yi Yan, yanyi@gig.ac.cn

Abstract

The eastern Himalayan syntaxis, where the Yarlung Tsangpo sharply bends, is one of the areas experiencing most rapid exhumation on Earth. The rapid exhumation is often regarded as the result of capture of the Yarlung Tsangpo by the Brahmaputra River. However, both the timing of integration of the Yarlung Tsangpo-Brahmaputra River and initiation of the rapid syntaxial exhumation are debated. As the ultimate sedimentary trap of the Yarlung Tsangpo-Brahmaputra River, the Nicobar Fan is a window to look into the drainage evolution and exhumation history of the eastern Himalaya. International Ocean Discovery Program Expedition 362 drilled the Nicobar Fan for the first time, recovering fan sediments dating back to the Early Miocene (~19 Ma). We apply trace elements and Sr-Nd isotopes to investigate the provenance of the sediments in the Nicobar Fan with the aim of constraining the timing of integration of the Yarlung Tsangpo-Brahmaputra River and initiation of the rapid syntaxial exhumation. The geochemical and Sr-Nd isotope compositions indicate an eastern Himalayan source dominated by the Greater Himalaya, with significant Gangdese arc contribution and primarily carried by the Brahmaputra River. Flux of Gangdese arc material appears to have been continuous from the base of the Nicobar Fan, suggesting that the Yarlung Tsangpo-Brahmaputra River has been established at least since ~19 Ma. Synchronously with the sharp rise in sedimentation rate, the abrupt change of geochemical and isotope compositions at ~9.2 Ma indicates an increase in erosion of the Greater Himalaya as the result of initiation of rapid exhumation in the broad syntaxial region. The proportion of Greater Himalayan material increased again at 3.5–1.7 Ma, consistent with a younger pulse of rapid exhumation focused in the core of the syntaxis since ~3.5 Ma. Our results show that initiation of the rapid syntaxial exhumation postdated integration of the Yarlung Tsangpo-Brahmaputra River by at least ~10 m.y. Therefore, tectonic uplift rather than river capture could be responsible for the initiation of the rapid syntaxial exhumation.

Key words: Nicobar Fan, Yarlung Tsangpo-Brahmaputra River, eastern Himalayan syntaxis, sedimentary record, International Ocean Discovery Program Expedition 362

1. Introduction

Collisional tectonics induces topographic variation and results in drainage reorganization via mechanisms such as river capture, diversion and reversal (e.g. Brookfield, 1998; Clark et al., 2004). Drainage reorganization markedly affects the distribution and intensity of erosion over an orogen, which in turn influences the style and location of crustal deformation (Cina et al., 2009). Therefore, study of drainage evolution during collisional orogeny is crucial to understanding the complex interplay between tectonic deformation and surface erosion (e.g. Bracciali et al., 2015). The Himalayan orogen, where active collision is ongoing and major South Asian rivers originate, is an ideal place in which to recognize tectonic-erosion interactions. The eastern Himalayan syntaxis is one of the most active tectonic regions on Earth and characterized by very rapid rock uplift and exhumation (Burg et al., 1997; Ding et al., 2001) (Fig. 1). The Yarlung Tsangpo runs eastward along the suture between the Himalaya and the Lhasa block, and then sharply bends southward through the eastern syntaxis, carving one of the world's largest and deepest gorges, the Yarlung Tsangpo Gorge. Downstream of the gorge, the Yarlung Tsangpo is called the Siang River and becomes the southwestward-flowing Brahmaputra River in the Himalayan foreland. It then meets the Ganges River, and finally discharges into the Bay of Bengal and the northeastern Indian Ocean, where it accumulates as the Bengal-Nicobar Fan system (Fig. 1). The sediments are now transferred to the Bengal Fan by turbidite currents via the Swatch-of-No-Ground submarine canyon and the Active Channel (Fig. 1) which has been active since 12.5 ka BP, however, there were probably more than one canyon-channel system at times before then (Curray et al., 2003). The Bengal-Nicobar Fan system extends southward for over 3000 km to ~7°S and covers an area of $\sim 4\times10^6$ km^2 with a volume of $>8\times10^6$ km^3 since ca. 20 Ma (Curray et al., 2003, Pickering et al., 2020). As the ultimate sediment trap of the Ganges River and Yarlung Tsangpo-Brahmaputra River, the Bengal-Nicobar Fan preserves records of Himalayan erosion and is therefore vital to deciphering the drainage evolution and exhumation history of the eastern Himalaya.

The eastern Himalayan syntaxis presently feeds 45–70% of the bulk sediment flux of the Brahmaputra River, suggesting an exhumation rate up to 10 mm/yr or more (e.g. Singh and France-Lanord, 2002; Bracciali et al., 2016). Such high exhumation rates are also supported by the bedrock cooling age as young as <1 Ma (e.g. Seward and Burg, 2008). To explain the extremely rapid syntaxial exhumation, most researchers emphasize the role of tectonics caused by northward indentation of the northeastern corner of the Indian plate into Eurasia, which leads to growth of the syntaxis (e.g. Burg et al., 1997; Seward and Burg, 2008; Bendick and Ehlers, 2014). However, the "tectonic aneurysm" model highlights the potential coupling between tectonics and erosion and associates the rapid exhumation with the incision of the Yarlung Tsangpo Gorge (Zeitler et al., 2001, 2014). This model suggests that rapid, focused erosion weakens the upper crust, leading to lower crustal flow into the weakened zone, and promoting the doming of the upper crust, thus generating a self-sustaining feedback between tectonic deformation and surface erosion (Zeitler et al., 2001). This model also suggests that initiation of the rapid syntaxial exhumation could be triggered by capture of the Yarlung Tsangpo by the Brahmaputra River (Zeitler et al., 2001). However, both the timing of integration of the Yarlung Tsangpo-Brahmaputra River and initiation of the rapid syntaxial exhumation continue to be debated (e.g. Bracciali et al. 2015, 2016; Najman et al., 2019).

It has been proposed that the Yarlung Tsangpo flowed southeastward into the Irrawaddy River through the Parlung Tsangpo, before it was captured by the Siang-Brahmaputra River at ~10 Ma (Brookfield, 1998) or 3–4 Ma (Zeitler et al., 2001; Clark et al., 2004). The timing of this capture event was however estimated based on the proposed age of the localized uplift of the eastern syntaxis. Recent provenance analyses of the paleo-Brahmaputra deposits provide new time constraints on integration of the Yarlung Tsangpo-Brahmaputra River, to be either in the Late Miocene or the Early Miocene. The first appearance of Gangdese arc detritus, indicative of a Yarlung Tsangpo contribution, in the eastern Himalayan foreland basin were detected at ~10 Ma (Cina et al., 2009), at ~7 Ma (Chirouze et al., 2013) and in the Early Miocene (Lang and Huntington, 2014) in various sections. Meanwhile, Bracciali et al. (2015) observed the first influx of Gangdese arc material in Lower Miocene sediments of the Surma Basin (northeastern Bengal Basin) downstream of the Brahmaputra River. The timing of onset of the rapid syntaxial exhumation remains poorly constrained, varying from the Late Miocene to the Plio-

Pleistocene (11–2 Ma). Most of the bedrock thermochronology data from the syntaxial region show young cooling ages and indicate onset of rapid exhumation since ~3.5 Ma (e.g. Burg et al., 1997; Seward and Burg, 2008). However, bedrock zircon U-Pb geochronology denoted local melting accompanying rapid cooling since ~11–9.7 Ma (Ding et al., 2001; Booth et al., 2004). A synthesis study of cooling history within and around the syntaxis indicates a significant pulse of rapid exhumation at 10–5 Ma (Zeitler et al., 2014). The paleo-Brahmaputra detrital records could offer a long-term exhumation history of the syntaxis after the integration of the Yarlung Tsangpo-Brahmaputra River, which avoids problems associated with study of the syntaxis bedrock where erosion and metamorphism have removed or obscured the early exhumation history. However, estimates of the onset of rapid exhumation interpreted from detrital thermochronology are also variable. Rapid exhumation was recorded in the eastern Himalayan foreland basin by 7–5 Ma (Lang et al., 2016), in the Surma Basin since ~3.5–2 Ma (Bracciali et al. 2016) and in the Bengal Fan since ~3.5 Ma (Najman et al., 2019), as indicated by the first occurrence of detrital minerals with short lag times.

International Ocean Discovery Program (IODP) Expedition 362 successfully cored Nicobar Fan sediments dating back to the Early Miocene (~19 Ma) (Fig. 1). These sediments represent a key sedimentary archive of eastern Himalayan evolution (McNeill et al., 2017a, 2017b). The Nicobar Fan sediments was transported for a long distance over 1700 km from the outlet. Therefore, compared to the proximal records of the fluvial-deltaic Himalayan foreland basin and Surma Basin, the Nicobar Fan sediments might be expected to minimize local effects that would obscure the upstream signal, and also provide a continuous marine sedimentary succession with better depositional age constraints. Evidence from the Bengal Basin and the Bay of Bengal indicates that the Ganges River and the Brahmaputra River entered the Bay of Bengal separately at some time in the past (e.g. Curray et al. 2003; Govin et al., 2018), rather than merging together before entering the bay as they do today. Therefore, compared to the Bengal Fan, the Nicobar Fan in the east should be less influenced by the signal of the Ganges River that drains the central Himalaya and peninsular India. Any significant contribution from the Irrawaddy River to the Nicobar Fan is unlikely as it requires transfer of the sediments across the forearc to the west, which was restricted by the then exposed Yadana-M8 Highs and the uplifted Sewell-Alcock Rises west of the Andaman Sea (Racey and Ridd, 2015) (Fig. 1). Sediment isopaches of the Cenozoic Martaban basin in the Andaman Sea related to the development of the Salween-Irrawaddy delta also show no significant sediment transfer to the west (Racey and Ridd, 2015) (Fig. 1). Because the Himalayan units and the Gangdese arc have contrasting lithologies and geochemistry (e.g. Singh et al., 2008; Wu et al., 2010) (Table 1), we conduct a provenance analysis of the Nicobar Fan sediments using trace elements and Sr-Nd isotope composition. Specifically, we aim to constrain the timing of integration of the Yarlung Tsangpo-Brahmaputra River by detecting the first appearance of Gangdese arc material, and attempt to estimate the timing of initiation of rapid exhumation of the eastern Himalayan syntaxis from the perspective of a provenance shift. Lastly, we evaluate the interaction between the rapid syntaxial exhumation and the Yarlung Tsangpo-Brahmaputra River evolution.

2. Background

2.1. Tectonic setting of the eastern Himalaya

The collision between the Indian and Eurasian plates, beginning at 65–43 Ma, deformed and uplifted the northern margin of the Indian continent to form the Himalayan orogen (Yin, 2006). The Himalaya is separated from the Lhasa block of the Eurasian plate by the Indus-Yarlung Suture Zone (Fig. 1). The southern Lhasa block is intruded by Cretaceous–Paleogene magmatic and volcanic rocks of the Andean-type Gangdese arc, resulting from the northward subduction of the Tethyan Ocean (e.g. Copeland et al., 1995). South of the suture, the Himalaya is classically divided into four lithotectonic units: the Tethyan Himalaya (Paleoproterozoic–Eocene sedimentary cover), the Greater Himalaya (medium- to high-grade Paleoproterozoic–Ordovician metamorphic crystalline rocks), the Lesser Himalaya (Proterozoic–Cambrian metasedimentary and sedimentary rocks) and the Sub-Himalaya (Cenozoic foreland basin sediments) (Yin, 2006) (Fig. 1). Rapid exhumation of the Greater Himalaya at the rate of 2–5 mm/yr initiated at ~23 Ma, associated with movement on the Main Central Thrust and the South Tibetan Detachment System (Fig. 1), and ceased around 18–16 Ma in the western and central Himalaya and around 14–10 Ma in the eastern Himalaya (Najman et al., 2019 and references therein). The Gangdese arc shows significantly higher ε_{Nd} and lower $^{87}Sr/^{86}Sr$ than the Himalayan units, while the Lesser Himalaya have the lowest ε_{Nd} and most radiogenic $^{87}Sr/^{86}Sr$ among the Himalayan units (Singh et al., 2008; Wu et al., 2010) (Table 1).

The eastern Himalayan syntaxis is mainly composed of high-grade metamorphic crystalline rocks of the Greater Himalaya, which forms the peak of Namche Barwa (7782 m) in the core of the syntaxis (Ding et al., 2001). The syntaxis is a north-plunging antiformal and in part domal structure (Bracciali et al., 2016). The Greater Himalaya in the syntaxis shared a similar tectonothermal history with that in the main belt of the

Himalaya before their evolution diverged in the Late Miocene (Najman et al., 2019). Thereafter, the Greater Himalaya showed younger metamorphism and more rapid exhumation (up to 10 mm/yr or more) in the syntaxis. Along the sharply curved eastern Himalayan syntaxis, the WNW-ESE trending Himalayan collisional belt passes abruptly into the N-S striking Indo-Burman Ranges (Fig. 1). The Indo-Burman Ranges is divided laterally into two portions. The Neogene Indo-Burman Ranges in the west represent Himalayan-derived Bengal-Nicobar Fan sediments incorporated into the accretionary prism, whereas the Paleogene Indo-Burman Ranges in the east were interpreted as forearc sediments equivalent to the Central Myanmar Basin or trench sediments with significant input from the Burmese arc (including the Wuntho-Popa Arc and the Cretaceous–Paleogene plutons intruding the Mogok Metamorphic Belt) (Allen et al., 2008). The Burmese arc overall shows similar Sr-Nd isotope compositions to the Gangdese arc (Wu et al., 2010; Lin et al., 2019) (Table 1).

2.2.Litho-stratigraphy and age model of the Nicobar Fan

The Nicobar Fan is separated from the Bengal Fan by the Ninetyeast Ridge (formed from 77 to 43 Ma, Frey et al., 2015) and now being subducted beneath the Sumatra margin. IODP Expedition 362 drilled two sites on the northern Nicobar Fan east of the Ninetyeast Ridge in 2016, recovering the complete sedimentary succession at Site U1480 to a basement depth of 1415.53 meter below seafloor (mbsf), and from 1149.7 mbsf to within 10s m of basement at 1500 mbsf at Site U1481 (McNeil et al., 2017a) (Figs. 1 and 2). At Site U1480, Units I–IIIA (0–1310.02 mbsf) represent the Nicobar Fan and are composed predominantly of siliciclastic sediment gravity-flow deposits (mostly turbidities) like the Bengal Fan (McNeil et al., 2017a). Unit I is 26.42 m-thick, and contains calcareous mud and interbeds of fine sand and mud. Unit II (1223.93 m-thick) is characterized by frequent occurrence of fine sand and sandy silt alternating with mud and is divided into three subunits. Unit IIIA is only 59.67 m-thick and contains gray-green and minor reddish-brown mudstone with rare thin-bedded siltstone, representing the earliest depositional phase of the fan. At Site U1481, the upper ~210 m of the sedimentary succession is equivalent to Unit IIC at Site U1480, while the lower ~140 m corresponds to Unit IIIA but includes a ~20 m-thick bed of fine-grained sandstone and siltstone at its base (McNeil et al., 2017a).

The shipboard age models of Expedition 362 sites were generated using microfossils (McNeil et al., 2017a). Backman et al. (2019) later proposed a revised age model of Site U1480 taking post-cruise biostratigraphic data into account. According to the above age models, the base of the Nicobar Fan at Site U1480 (1250.35 mbsf) is estimated at ~15.3 Ma, however, the lowest Nicobar Fan sediments (1500 mbsf) at Site U1481 is estimated older at ~19.2 Ma (Fig. 2). Thicker Unit IIIA at Site U1481 with older and coarser siliciclastic sediments potentially reflects topographic variations, because the site is less proximal to the Ninetyeast Ridge and has deeper basement. At both sites, sedimentation rates increased dramatically and synchronously at ~9.2 Ma corresponding to the Units IIIA and IIC boundary (Fig. 2), from 8–15 m/m.y. to ~220 m/m.y. (Fig. 5). This timing was placed at ~9.5 Ma by McNeil et al. (2017b), but it should be ~9.2 Ma according to the age models of McNeil (2017a) and Backman et al. (2019). At Site U1480, the high sedimentation rate persisted, but decreased slightly to 65–125 m/m.y. at 5.9 Ma and subsequently increased to 290 m/m.y. at ~2.4 Ma (Fig. 5). The sedimentation rate then dropped to 3–42 m/m.y. since ~1.7 Ma (Units I and II boundary), which was interpreted as fan abandonment due to tectonic blocking of the sediment routing to the Nicobar Fan by the Ninetyeast Ridge as it collided with the Sunda margin (McNeil et al., 2017a).

3. Methods

We conducted trace element and Sr-Nd isotopic analyses on the bulk silicate fraction of the Nicobar Fan muds/mudstones, in an attempt to trace provenance variations. A total of sixty-eight core samples were collected (Fig. 2), primarily from the mud/mudstone of the upper part of turbidite beds. The samples were leached with 2N acetic acid to remove carbonates prior to element and isotopic analyses at the State Key Laboratory of Isotope Geochemistry, Guangzhou Institute of Geochemistry, Chinese Academy of Sciences. Trace elements of all the samples were measured on a Perkin-Elmer Sciex Elan 6000 inductively coupled plasma mass spectrometer (ICP-MS). Sr and Nd isotopic ratios of sixty samples were analyzed on a MicroMass Isoprobe multicollector inductively coupled plasma mass spectrometer (MC-ICP-MS). The $^{87}Sr/^{86}Sr$ ratios of thirteen samples could not be measured because we failed to separate Sr from these samples. Analytical methods are provided in full in Supplementary Materials.

4. Results

Results of the trace element and Sr-Nd isotopic analyses of the silicate fraction of the Nicobar Fan samples are listed in Supplementary Tables A.1 and A.2, respectively.

4.1.Trace elements

The trace elements Rb, Th, Ta, Nb, Y, show higher concentrations in our samples compared to the Upper Continental Crust (UCC) (Rudnick and Gao, 2003) (Fig. 3a). Abundances of transitional elements, V, Sc, Co, Cr and Ni in the Nicobar Fan samples are also higher than those of the UCC (Fig. 3a). Most samples share similar pattern of trace elements, except that Co and Ni abundances show a considerably scatter and are significantly higher in Unit IIIA than in Units I and II. In general, trace elements in the Nicobar Fan samples show similar characteristics to those in the Himalayan-derived Neogene Surma Basin and Bengal Fan sediments (Hossain et al., 2010; Crowley et al., 1998), although Ta, Zr and Hf concentrations in the Surma Basin sediments are obviously higher than those in the Nicobar Fan samples (Fig. 3a). Chondrite-normalized distribution patterns of rare earth element (REE) concentrations in the Nicobar Fan samples are similar to those of the UCC, as well as Neogene Surma Basin and Bengal Fan sediments, in displaying light REEs enrichment, heavy REEs depletion and a negative Eu anomaly (Fig. 3b). Temporal variations of element contents and ratios however show an abrupt change at ~9.2 Ma (boundary of Units II and IIIA) at both Sites U1480 and U1481, characterized by marked rise in Th, Ta and Nb contents and La/Lu and La_N/Yb_N ratios but significant drop in Cr/Th ratio (Fig. 4). Although highly variable in terms of these element contents and ratios since ~9.2 Ma, the Unit II sediments overall show higher Th, Ta and Nb contents, higher La/Lu and La_N/Yb_N ratios but lower Cr/Th ratio than those of the Unit IIIA sediments.

4.2.Sr and Nd isotopes

The $^{87}Sr/^{86}Sr$ ratios of the Nicobar Fan samples vary from 0.719718 to 0.750453 (Table A.2). The Unit IIIA sediments show relatively uniform $^{87}Sr/^{86}Sr$ ratios ranging from 0.721300 to 0.731113 (average of 0.726131), which then increased rapidly and concurrently by 0.03 units after ~9.2 Ma (the Units II and IIIA boundary) at both Sites U1480 and U1481 (Fig. 5). Although highly variable between 0.723152 and 0.750453, the $^{87}Sr/^{86}Sr$ ratios of the Unit II sediments (average of 0.734478) are generally higher than those of the Unit IIIA sediments. However, the Unit I sediments have an average $^{87}Sr/^{86}Sr$ ratios of 0.722044, close to the Unit IIIA average.

The ε_{Nd} values range from -16.1 to -7.8 (Table A.2), and the temporal evolution is negatively correlated with the $^{87}Sr/^{86}Sr$ ratios (Fig. 5). The Unit IIIA sediments have higher ε_{Nd} values, ranging from -13.3 to -7.8 (average of -11.7), whereas the Unit II sediments generally have lower ε_{Nd} values (average of -13.5) highly oscillating between -16.1 and -10.5. An oscillatory decrease in ε_{Nd} values is observed around the Units II and IIIA boundary (Fig. 5). The ε_{Nd} values decreased from -12.2 at 9.24 Ma to -14.7 at 8.76 Ma at Site U1480, while it first increased from -11.9 at 9.26 Ma to -10.1 at 9.18 Ma but then dropped to -14.8 at 8.72 Ma at Site U1481. The ε_{Nd} values of the Unit I samples are concentrated in the range of -11.5 to -10.6 (average of -11.1).

The Nicobar Fan sediments overall exhibit negative correlations between ε_{Nd} versus Th, Ta and Nb contents and La/Lu and La_N/Yb_N ratios, and a positive correlation between ε_{Nd} versus Cr/Th ratio (Fig. 6). Because Nd isotopes are not modified by mineral sorting processes, we deduce that these trace element contents and ratios are not significantly affected by mineral sorting but primarily controlled by the composition of the source areas (the Himalaya and the Gangdese arc as discussed below).

5. Discussion

5.1.Eastern Himalayan Provenance for the Nicobar Fan sediments

The trace element and REE distribution patterns of the Nicobar Fan sediments denote a Himalayan provenance dominated by sedimentary-metasedimentary rocks. However, enrichment of the transitional elements relative to UCC indicates additional input of more mafic rocks. The Niocbar Fan sediments also reflect mixing between felsic and intermediate sources on a plot of Cr/Th versus Th/Sc (Fig. A.1). It is also noteworthy that the Nicobar Fan sediments show higher ε_{Nd} values and lower $^{87}Sr/^{86}Sr$ ratios than contemporary sediments in the Bengal Fan (France-Lanord et al., 1993; Galy et al., 1996; Galy et al., 2010), the Nepalese foreland (Huyghe et al., 2001, 2005; Szulc et al., 2006), and the eastern Himalayan foreland (Chirouze et al., 2013) through the Neogene (Fig. 5). The fan sediments also have higher ε_{Nd} values and lower $^{87}Sr/^{86}Sr$ ratios than the Surma Basin sediments in the Miocene (Bracciali et al., 2015) (Fig. 5). Here we employ a Sr-Nd isotope diagram to distinguish the possible sources for the Nicobar Fan (Fig. 7a). To understand the source-to-sink process from the Himalaya to the northeastern Indian Ocean, we also compare Sr-Nd isotope compositions of the Nicobar Fan sediments with those of modern sediments in the Ganges and Brahmaputra mainstreams upstream their confluence in the Bengal delta (Singh and France-Lanord, 2002; Singh et al., 2008).

The Brahmaputra sediments have obviously higher ε_{Nd} values and lower $^{87}Sr/^{86}Sr$ ratios than the Ganges sediments (Table 1). They are separate from each other in the Sr-Nd isotope diagram (Fig 7a). Such distinction reflects contributions from their drainage basins. The Ganges River drains the central Tethyan, Greater and Lesser Himalayas as well as peninsular India. Of these, the Greater and Lesser Himalayas make up most of the sediment load of the Ganges River, with the Greater Himalaya contributing >65% of the total (Singh et al., 2008). Sediment input from the Tethyan Himalaya lying in the rain shadow and from peninsular India is estimated to be minor (Singh et al., 2008). The Brahmaputra River drains the same units in the eastern Himalaya, with its upper reach, the Yarlung Tsangpo, draining the Tethyan Himalaya and the Gangdese arc. Therefore, the Brahmaputra River is characterized by significant input from the Gangdese arc, whereas the Ganges River shows more input from the Lesser Himalaya (Fig 7a). The Sr-Nd isotope compositions of the Nicobar Fan sediments are close to the field of the Brahmaputra sediments with slightly higher ε_{Nd} values (Fig 7a), showing Greater Himalayan affinity plus a significant Gangdese arc contribution, which could account for enrichment of the transitional elements.

Although the Burmese arc has similar Sr-Nd isotope compositions to the Gangdese arc (Table 1 and Fig 7a), it could not be the major contributor to the arc components in the Nicobar Fan. Direct input from the Burmese arc to the Nicobar Fan is unlikely, because the accretionary prism (the Paleogene Indo-Burman Ranges) was uplifted and emerged around 39–37 Ma, as evidenced by the quasi-closed estuarine condition and the shift from westward-directed deltaic system to southward-directed fluvial-deltaic system in the forearc basin (the western Central Myanmar Basin) at that time (Licht et al., 2016;

2018). The Paleogene Indo-Burman Ranges would thus have provided a barrier to transport of the Burmese arc material westward. Therefore, during the Neogene, the Burmese arc material would have been delivered by the Irrawaddy River flowing southward along the Central Myanmar Basin and finally been trapped in the Martaban Basin (Racey and Ridd, 2015). Although sediments from the arc-derived Paleogene Indo-Burman Ranges were regarded as a significant contributor to the eastern Bay of Bengal in the last glacial-interglacial cycle when the eastern Bengal Fan was inactive, they were speculated to be transported by ocean surface currents driven by monsoon winds (e.g. Colin et al., 1999; Joussain et al., 2016). The Nicobar Fan was active during 19–1.7 Ma and dominated by sandy and muddy turbidites (Pickering et al., 2020), which were primarily advected by turbidite currents instead of surface currents. It is obvious that the small rivers draining the western flank of the Indo-Burman Ranges could not supply turbidites to the distant Nicobar Fan sites. Moreover, the anticyclonic/cyclonic surface circulation driven by summer/winter monsoons in the Bay of Bengal are restricted north of 12°N (e.g. Joussain et al., 2016). We thus do not expect that the Paleogene Indo-Burman Ranges material would reach the Nicobar Fan sites near the Equator today and in the Southern Hemisphere during the Miocene (Hall, 2012) (Fig. 8). Therefore, we exclude that the arc components in the Nicobar Fan were recycled from the Paleogene Indo-Burman Ranges.

The Nicobar Fan sediments also overlap the range of Neogene sediments in the Surma Basin which represent the paleo-Brahmaputra deposits (Bracciali et al., 2015). The close affinity in Sr-Nd isotope compositions between the Nicobar Fan, the Surma Basin and the Brahmaputra sediments implies that the Nicobar Fan sediments were primarily supplied by the Brahmaputra River from the eastern Himalaya. Unlike the Nicobar Fan sediments, Sr-Nd isotope compositions of the Bengal Fan sediments overlap both the ranges of the Brahmaputra and the Ganges sediments (Fig. 7a), indicating a mixture of sediments derived from the two rivers. The Nepalese foreland sediments have most affinity with the Ganges sediments, displaying significant Lesser Himalaya input, as expected (Fig. 7a). Mixing of the Ganges and Brahmaputra sediments in various proportions in the Bengal Fan during the Neogene has also been demonstrated by detrital zircon U-Pb dating from Bengal Fan IODP sites (Blum et al., 2018). In light of the temporal variation in detrital U-Pb age populations, the Ganges River is known to have served as the major source of sediment to the Bengal Fan prior to ~3.5 Ma, although it is nowadays mostly supplied by the Brahmaputra River (Blum et al., 2018). The difference in Sr-Nd isotope compositions between the Bengal Fan and the Nicobar Fan sediments implies that the Ganges and the Brahmaputra Rivers used to deliver sediments separately to the Bay of Bengal through independent river mouths and slope canyon-channel systems (Fig. 8). Mixing of Ganges and Brahmaputra sediments by channel avulsions appears to have been common in the Bengal Fan, but not in the Nicobar Fan, or the Nicobar Fan sediments would also plot between the Ganges and the Brahmaputra sediments in the Sr-Nd isotope diagram. Separation of the Ganges-Brahmaputra river mouths is evidenced by a paleo-Brahmaputra course east of the Shillong Plateau, which was redirected west by the rising plateau and the westward-propagated Indo-Burman Ranges at 5.2–4.9 Ma (Govin et al., 2018) (Figs. 8b and 8c). However, it remains unknown when the two rivers first joined after then as river avulsion might occurred frequently. Some clues indicate that the Ganges-Brahmaputra River mouths were still separated at times during the Quaternary. For example, distribution of the Bengal Fan sequences suggests two active canyon-channel systems during 1.9–0.96 Ma (Curray et al., 2003), which were probably fed by the Ganges River and Brahmaputra River respectively. Therefore, compared to the Bengal Fan, the Nicobar Fan provides a simpler erosion record of the eastern Himalaya that can be used to constrain the timing of integration of the Yarlung Tsangpo-Brahmaputra River and initiation of the rapid syntaxial exhumation.

5.2. An integrated Yarlung Tsangpo-Brahmaputra River since Early Miocene

The Sr-Nd isotope compositions of the Nicobar Fan sediments indicate an eastern Himalayan source dominated by the Greater Himalaya but with significant Gangdese arc contribution since ~19 Ma. It is noteworthy that the arc component in Unit IIIA is stronger than that in Unit II, as indicated by the significantly higher Co and Ni contents (Fig. 3a), lower Th, Ta and Nb contents, lower La/Lu and La_N/Yb_N ratios and higher Cr/Th ratios (Fig. 4), as well as higher ε_{Nd} values and lower $^{87}Sr/^{86}Sr$ ratios (Figs. 5 and 7). The Unit IIIA sediments also show higher ε_{Nd} values (-13.3 to -7.8) than modern Brahmaputra sediments (-16.9 to -12.5) (Fig. 7a). Because Gangdese arc material in the Brahmaputra River is presently strongly diluted by the Greater Himalayan detritus derived from the rapidly exhuming eastern Himalayan syntaxis, the higher ε_{Nd} values seen in Unit IIIA sediments at 19–9.2 Ma could reflect the Brahmaputra sedimentation prior to rapid syntaxial exhumation. Determining the proportions of the Greater Himalaya and the Gangdese arc contributing to the Nicobar Fan might be complex, because the Lesser and Tethyan Himalayas would be part of the source mixture although their contributions are minor. Nevertheless, we perform a simple two-components mixing model based on Sr-Nd isotopes only regarding the Greater Himalaya and the Gangdese arc (Fig. 7b). In this model, the proportion of the Gangdese arc material could be over ~50% in average in the Unit IIIA sediments (Fig. 7b).

Airfall volcanic ash is occasionally found through Unit IIIA in form of very thin (0.5–4 cm) ash layers (McNeill et al., 2017a), but we avoided collecting samples from these layers. Except for a single sample (~16.7 Ma) with a high ε_{Nd} value (-7.8) (Fig. 5), the Unit IIIA sediments show relatively stable $^{87}Sr/^{86}Sr$ ratios, ε_{Nd} values and element concentrations and ratios at both Sites U1480 and U1481, indicating a long-term continuous input from the Gangdese arc and no significant dispersed volcanic ash in the samples. Moreover, the sample with a high ε_{Nd} value (-7.8) was collected from silty mudstone within turbidite units, which obviously lack of volcanic ash. All the evidence above suggests that igneous detritus instead of volcanic ash is responsible for the geochemical characteristic of the Unit IIIA sediments.

The influence of Gangdese arc detritus in the Nicobar Fan is also supported by the presence of typical Cretaceous–Eocene Gangdese zircons (Govin et al., 2018) throughout the core samples, with the proportion of <150 Ma population ranging 2–17% (McNeil et al., 2017b) (Fig. 5). The oldest sediments (~18 Ma) in Site U1451 on the Bengal Fan also show 8% zircon grains of <150 Ma population (Blum et al., 2018). As the 75–50 Ma population is absent in the Himalayan units and rare in the Bomi-Chayu batholith east of the syntaxis, it can be regarded as an exclusive indicator of the Gangdese arc (Bracciali et al., 2015; Lang and Huntington, 2014). This age population is found in the Nicobar Fan sediments, particularly in the Lower Miocene sample, although only at <6% of the total population (Fig. 5). Therefore, the detrital geochronology, along with our Sr-Nd isotope results, show long-term continuous input from the Gangdese arc to the Nicobar Fan via the Brahmaputra River. We thus propose an integrated Yarlung Tsangpo-Brahmaputra River being active at least since the Early Miocene (~19 Ma) (Fig. 8a). This timing is compatible with the results from the eastern Himalayan foreland near the Siang River (Lang and Huntington, 2014) and from the Surma Basin (Bracciali et al., 2015), suggesting connection of the Yarlung Tsangpo-Brahmaputra River through the Siang River. Importantly, we provide improved age constraints because the depositional age of the fluvial deposits is difficult to accurately determine. Our result also demonstrates the diachronous arrival of Gangdese arc detritus in the eastern Himalayan foreland, which was dated as ~10 Ma in the Subansiri River section (Cina et al., 2009), ~7 Ma in the Kameng River section (Chirouze et al. 2013) and ~5 Ma farther west (Govin et al., 2018), arose from the westward migration of the Brahmaputra course (Govin et al., 2018). However, whether and when the Yarlung Tsangpo was captured by the Brahmaputra River remains ambiguous. Bracciali et al. (2015) found no detrital zircons of Gangdese-age in two Upper Eocene–Oligocene samples in the Surma Basin. Based on the sedimentary records in the Central Myanmar Basin, Robinson et al. (2014) proposed that a Yarlung Tsangpo-Irrawaddy River was established by 40 Ma and was then captured by the Brahmaputra River before the Early Miocene. In contrast, Licht et al. (2016) found no evidence to support a Yarlung Tsangpo-Irrawaddy connection. This might infer a long-lived Yarlung Tsangpo-Brahmaputra River that was established before the Early Miocene, and it is possible that the Brahmaputra River drained east of the Surma Basin at that time.

5.3. Two-stage rapid exhumation of the eastern Himalayan syntaxis since Late Miocene

The noteworthy increase in sedimentation rate at the Nicobar Fan sites at ~9.2 Ma was interpreted as the result of the reduction in accommodation space of the Bengal Basin due to the inversion of the Shillong Plateau and the westward encroachment of the Indo-Burma Ranges, which increased sediment supply directly to the Nicobar Fan (McNeil et al., 2017b). However, although the exhumation of the Shillong Plateau begun at 15−9 Ma (Biswas et al., 2007), topographic growth of the plateau was chronologically decoupled from the exhumation and did not initiate until 5.2–4.9 Ma (Govin et al., 2018) owing to the contrasting erodibility between the sedimentary cover and the resistant basement rocks (Biswas et al., 2007). The growth history of the Indo-Burma Ranges has not yet been accurately dated. Thus, the sedimentation rate variation at ~9.2 Ma is hard to be interpreted as a reflection of the reduction in continental accommodation space. Synchronous with the acceleration in sedimentation rate, the abrupt change in trace element contents and ratios and Sr-Nd isotope compositions around 9.2 Ma denotes a provenance shift (Figs. 4 and 5). The decreasing ε_{Nd} values and increasing $^{87}Sr/^{86}Sr$ ratios implies increasing flux of Greater and/or Lesser Himalayan material compared to Gangdese arc sediments (Fig. 7a). Although the increase of Lesser Himalayan detritus in response to the Lesser Himalayan exhumation was proposed in the western and central Himalayan forelands at 12–10 Ma (Huyghe et al., 2001; Szulc et al., 2006), it has not yet been documented in the eastern Himalayan foreland. The Lesser Himalaya could not be the primary source leading to the sediment geochemistry and sedimentation rate changes of the Nicobar Fan at ~9.2 Ma. If that was the case then post-9.2 Ma sediments would show extremely low ε_{Nd} values and high $^{87}Sr/^{86}Sr$ ratios like the Nepalese foreland under such accelerating sedimentation rate (Fig. 7a).

Instead, we ascribe the changes in sediment geochemistry and sedimentation rate at ~9.2 Ma to an increase in the flux of Greater Himalayan material (the proportion increased from ~50% in Unit IIIA to ~70% in Unit II, Fig. 7b) linked to the rapid exhumation of the Greater Himalayan crystalline rocks in the eastern Himalayan syntaxis (Fig. 8b). This conclusion is also supported by the detrital apatite fission-track data from the Nicobar Fan; apatite grains with short (<1 m.y. and even zero) lag times indicating rapid source-area exhumation were observed at 9–2 Ma (Pickering et al., 2018). Initiation of rapid syntaxial exhumation as reflected in the Nicobar Fan sediments (~9.2 Ma) is consistent with the older onset ages, ~11–9.7 Ma (Ding et al., 2001; Booth et al., 2004) and ~10 Ma (Zeitler et al., 2014), determined from the bedrock thermochronology and geochronology. It is also compatible with the poorly dated constraints from detrital thermochronology from the foreland sections downstream the Siang River, of 7–5 Ma or earlier (Lang et al., 2016). Zeitler et al. (2014) proposed that rapid exhumation starting from ~10 Ma took place in a broad syntaxial region including the easternmost Lhasa block (Fig. 8b). The variations of the Sr-Nd isotope compositions and the sedimentation rate in Unit II suggest that the rapid syntaxial exhumation was likely to have reduced around 6–5 Ma (Fig. 5), in agreement with the model proposed by Zeitler et al. (2014).

An interval of very low ε_{Nd} values (-14 to -16) and high $^{87}Sr/^{86}Sr$ ratios (0.74 to 0.75) in the Nicobar Fan sediment is observed again at 3.5–1.7 Ma when sedimentation rates reached a peak of ~290 m/m.y. (Fig. 5) before Pleistocene fan abandonment. The proportion of the Greater Himalayan material increase up to ~80% (Unit IIA average in Fig. 7b). This episode is coeval with the previously proposed younger onset age of the syntaxial exhumation at ~3.5 Ma based on most of the bedrock thermochronology data (e.g. Burg et al., 1997; Seward and Burg, 2008). This younger pulse of rapid exhumation since ~3.5 Ma was stronger but only focused in the Namche Barwa massif, defined as the core of the syntaxis northeast of the Nam La Thrust (Zeitler et al., 2014) (Fig. 8c). It is also witnessed in the Bengal Fan and the Surma Basin, as evidenced by the presence of detrital minerals with <1 m.y. lag times since ~3.5 Ma (Najman et al., 2019; Bracciali et al. 2016). The absence of this signal of rapid syntaxial exhumation in the Bengal Fan between 9.2 and 3.5 Ma might be due to strong supply of the Ganges sediments to that depocenter (Blum et al., 2018). The variations in sediment geochemistry and sedimentation rate seen at ~9.2 Ma in the Nicobar Fan were not observed in the Bengal Fan sites either. The stronger exhumation pulse since ~3.5 Ma enabled more Brahmaputra sediments to be delivered into the Bengal Fan (Fig. 8c), as indicated by the increase of Gangdese-age zircons and the first appearance of short-lag time minerals (Blum et al., 2018; Najman et al., 2019). However, it is puzzling that the signal of rapid syntaxial exhumation did not appear until 3.5–2.0 Ma in the Surma Basin, at odds with the presence of Gangdese arc material since the Early Miocene (Bracciali et al., 2015, 2016). This mis-match might result from the effects of dilution, hydraulic sorting and grain size.

The sedimentary record from the Nicobar Fan favors a two-stage exhumation model of the eastern Himalayan syntaxis. Despite the sedimentation rate and provenance variations, more specific detrital thermochronological work needs to be done on the Nicobar Fan to test this model. Regardless of whether the rapid syntaxial exhumation initiated at ~9.2 Ma or ~3.5 Ma these times significantly postdated the integration of the Yarlung Tsangpo-Brahmaputra River before ~19 Ma. If the capture of the Yarlung

Tsangpo by the Brahmaputra River occurred it would be at least 10 m.y. older than the inception of rapid exhumation. Therefore, drainage capture followed by focused incision cannot be responsible for the initiation of the rapid syntaxial exhumation as proposed by the tectonic aneurysm model (Zeitler et al., 2001). Instead, the rapid exhumation must have been initiated by tectonic uplift driven by the northward indentation of the northeastern corner of the Indian Plate (e.g. Burg et al., 1997; Seward and Burg, 2008; Bendick and Ehlers, 2014), which also distorted the course of the antecedent Yarlung Tsangpo-Brahmaputra River. The rock uplift, probably coupled with monsoon precipitation, would have enhanced river incision. A positive feedback between tectonics and erosion would thus have been established. Therefore, we do not exclude the tectonic aneurysm model (Zeitler et al., 2001; 2004) as the primary mechanism for sustaining or accelerating rapid syntaxial exhumation.

6. Conclusions

We conducted a provenance study on well-dated Nicobar Fan sediments (19 Ma–Recent) using trace element and Sr-Nd isotopic methods. We provide new time constraints for integration of the Yarlung Tsangpo-Brahmaputra River and initiation of rapid exhumation of the eastern Himalayan syntaxis.

The trace element and REE distribution patterns of the Nicobar Fan sediments indicate a Himalayan provenance. The Sr-Nd isotope compositions of the Nicobar Fan sediments further show a close affinity with Brahmaputra sediments dominated by the Greater Himalayan material but also with significant contributions from the Gangdese arc, demonstrating that the Nicobar Fan sediments were primarily supplied by the Brahmaputra River from the eastern Himalaya. The geochemical and Sr-Nd isotope compositions of the lower part of the Nicobar Fan indicate long-term continuous input of Gangdese arc material to the deep sea, and therefore imply an integrated Yarlung Tsangpo-Brahmaputra River flowing at least since the Early Miocene (~19 Ma). Based on variations in sedimentation rate and provenance of the Nicobar Fan, we favor a two-stage rapid exhumation model of the eastern Himalayan syntaxis. The abrupt change in geochemical and isotope compositions synchronous with the acceleration in sedimentation rate at ~9.2 Ma indicates increasing flux of Greater Himalaya material in response to the rapid exhumation commencing across a wide region of the eastern Himalayan syntaxis. The very low ε_{Nd} values and high $^{87}Sr/^{86}Sr$ ratios at 3.5–1.7 Ma, accompanying the peak sedimentation rate, corresponds to a younger pulse of rapid exhumation focused in the core of the syntaxis since ~3.5 Ma. Because initiation of rapid syntaxial exhumation postdated the integration of the Yarlung Tsangpo-Brahmaputra River by at least 10 m.y., this must have been triggered by tectonic uplift instead of capture of the Yarlung Tsangpo by the Brahmaputra River. A positive feedback between tectonics and erosion would have been established subsequently.

Acknowledgements

This research used samples and data provided by the International Ocean Discovery Program (IODP). We appreciate Science Party of IODP Expedition 362, in particular the Co-Chief Scientists (McNeill L.C. and Dugan B.E.) and the Staff Scientist (Petronotis K.E.), for their efforts. We also thank the IODP staff and JOIDES Resolution crew for their contributions during the expedition. This research was financially supported by the National Natural Science Foundation of China (grant 41606068), research grants from the Key Special Project for Introduced Talents of Southern Marine Science and Engineering Guangdong Laboratory (Guangzhou) (GML2019ZD0202), the National Programme on Global Change and Air-Sea Interaction (GASI-GEOGE-02), and Innovation Academy of South China Sea Ecology and Environmental Engineering, Chinese Academy of Sciences (ISEE2020YB07), and the Research Fund Program of Guangdong Provincial Key Laboratory of Marine Resources and Coastal Engineering (grant GDKLMRCE1804). This is contribution IS-XXXX from GIGCAS. We thank Sun Shengling and Zhang Le for their help on the analyses in GIGCAS laboratories and thank Kutterolf Steffen for his helpful discussion. We are grateful to the editor and two anonymous reviewers for their valuable comments which have substantially improved the paper. All the data used in this paper are provided in Supplementary materials.

References

Allen, R., Najman, Y., Carter, A., Parrish, R., Bickle, M., Paul, M., Garzanti, E., Reisberg, L., Chapman, H., Vezzoli, G., Andò, S., 2008. Provenance of the Tertiary sedimentary rocks of the Indo-Burman Ranges, Burma (Myanmar): Burman arc or Himalayan-derived? J. Geol. Soc. London 165, 1045–1057. https://doi.org/10.1144/0016-76492007-143.

Backman, J., Chen, W., Kachovich, S., Mitchison, F., Petronotis, K., Yang, T., Zhao, X., 2019. Data report: revised age models for IODP Sites U1480 and U1481, Expedition 362， in: McNeill, L.C., Dugan, B., Petronotis, K.E., the Expedition 362

Scientists, Sumatra Subduction Zone. Proc. IODP, vol. 362. International Ocean Discovery Program, College Station, TX. https://doi.org/10.14379/iodp.proc.362.202.2019.

Bendick, R., Ehlers, T.A., 2014. Extreme localized exhumation at syntaxes initiated by subduction geometry. Geophys. Res. Lett. 41(16), 5861–5867.

Biswas, S., Coutand, I., Grujic, D., Hager, C., Stöckli, D., Grasemann, B., 2007. Exhumation and uplift of the Shillong plateau and its influence on the eastern Himalayas: New constraints from apatite and zircon (U-Th-[Sm])/He and apatite fission track analyses. Tectonics 26, TC6013.

Blum, M., Rogers, K., Gleason, J., Najman, Y., Cruz, J., Fox, L., 2018. Allogenic and autogenic signals in the stratigraphic record of the deep-sea Bengal Fan. Sci. Rep. 8, 7973.

Booth, A.L., Zeitler, P.K., Kidd, W.S.F., Wooden, J., Liu, Y.P., Idleman, B., Hren, M., Chamberlain, C.P., 2004. U-Pb zircon constraints on the tectonic evolution of southeastern Tibet, Namche Barwa area. Am. J. Sci. 304, 889–929.

Bracciali, L., Najman, Y., Parrish, R.R., Akhter, S.H., Millar, I., 2015. The Brahmaputra tale of tectonics and erosion: Early Miocene river capture in the eastern Himalaya. Earth Planet. Sci. Lett. 415, 25–37.

Bracciali, L., Parrish, R.R., Najman, Y., Smye, A., Carter, A., Wijbrans, J.R., 2016. Plio-Pleistocene exhumation of the eastern Himalayan syntaxis and its domal 'pop-up'. Earth-Sci. Rev. 160, 350–385.

Brookfield, M.E., 1998. The evolution of the great river systems of southern Asia during the Cenozoic India-Asia collision: Rivers draining southwards. Geomorphology 22,

285–312.
Burg, J.P., Davy, P., Nievergelt, P., Oberli, F., Seward, D., Diao, Z., Meier, M., 1997. Exhumation during crustal folding in the Namche-Barwa syntaxis. Terra Nova 9, 53–56.
Chirouze, F., Huyghe, P., van der Beek, P., Chauvel, C., Chakraborty, T., Dupont-Nivet, G., Bernet, M., 2013. Tectonics, exhumation, and drainage evolution of the eastern Himalaya since 13 Ma from detrital geochemistry and thermochronology, Kameng River Section, Arunachal Pradesh. Geol. Soc. Am. Bull. 125(3–4), 523–538.
Cina, S.E., Yin, A., Grove, M., Dubey, C.S., Shukla, D.P., Lovera, O.M., Kelty T.K., Gehrels G.E., Foster D.A., 2009. Gangdese arc detritus within the eastern Himalayan Neogene foreland basin: Implications for the Neogene evolution of the Yalu-Brahmaputra river system. Earth Planet. Sci. Lett. 285(1–2), 0–162.
Clark, M.K., Schoenbohm, L.M., Royden, L.H., Whipple, K.X., Burchfiel, B.C., Zhang, X., Tang, W., Wang, E., Chen, L., 2004. Surface uplift, tectonics, and erosion of eastern Tibet from large-scale drainage patterns. Tectonics 23(1), TC1006.
Colin, C., Turpin, L., Bertaux, J., Desprairies, A., Kissel, C., 1999. Erosional history of the Himalayan and Burman ranges during the last two glacial–interglacial cycles. Earth Planet. Sci. Lett. 171(4), 647–660.
Copeland, P., Harrison, T.M., Pan, Y., Kidd, W., Roden, M., Zhang, Y., 1995. Thermal evolution of the Gangdese batholith, southern Tibet: a history of episodic un-roofing. Tectonics 14, 223–236.
Crowley, S.F., Stow, D.A.V., Croudace, I.W., 1998. Mineralogy and geochemistry of Bay of Bengal deep-sea fan sediments, ODP Leg 116: evidence for an Indian

subcontinent contribution to distal fan sedimentation, in: Cramp, A., MacLeod, C.J., Lee, S.V., Jones, E.J.W. (Eds.), Geological Evolution of Ocean Basins: Results from the Ocean Drilling Program. Geol. Soc. London Spec. Publ. 131, 151–176.

Curray, J.R., Emmel, F.J., Moore, D.G., 2003. The Bengal Fan: morphology, geometry, stratigraphy, history and processes. Mar. Petrol. Geol. 19(10), 1191–1223.

Ding, L., Zhong, D., Yin, A., Kapp, P., Harrison, T.M., 2001. Cenozoic structural and metamorphic evolution of the eastern Himalayan syntaxis (Namche Barwa). Earth Planet. Sci. Lett. 192, 423–438.

France-Lanord, C., Derry, L., Michard, A., 1993. Evolution of the Himalaya since Miocene time: isotopic and sedimentological evidence from the Bengal Fan. Geol. Soc. London Spec. Publ. 74(1), 603–621.

Frey, F.A., Silva, I.G.N., Huang, S., Pringle, M.S., Meleney, P.R., Weis, D. 2015. Depleted components in the source of hotspot magmas: Evidence from the Ninetyeast Ridge (Kerguelen). Earth and Planetary Science Letters, 426, 293-304.

Galy, A., France-Lanord, C., Derry, L.A., 1996. The Late Oligocene-Early Miocene Himalayan belt constraints deduced from isotopic compositions of Early Miocene turbidites in the Bengal Fan. Tectonophysics 260(1–3), 109–118.

Galy, V., France-Lanord, C., Peucker-Ehrenbrink, B., Huyghe, P., 2010. Sr-Nd-Os evidence for a stable erosion regime in the Himalaya during the past 12 Myr. Earth Planet. Sci. Lett. 290(3–4): 0–480.

Govin, G., Najman, Y., Copley, A., Millar, I., van der Beek, P., Huyghe, P., Grujic D., Davenport J., 2018. Timing and mechanism of the rise of the Shillong Plateau in the Himalayan foreland. Geology 46 (3), 279–282.

doi: https://doi.org/10.1130/G39864.1

Hall, R., 2012. Late Jurassic–Cenozoic reconstructions of the Indonesian region and the Indian Ocean. Tectonophysics 570–571, 1–41. http://dx.doi.org/10.1016/j.tecto.2012.04.021.

Hossain, H.M.Z., Roser, B.P., Kimura, J.I., 2010. Petrography and whole-rock geochemistry of the Tertiary Sylhet succession, northeastern Bengal Basin, Bangladesh: Provenance and source area weathering. Sediment. Geol. 228(3–4), 171–183.

Huyghe, P., Galy, A., Mugnier, J. L., France-Lanord, C., 2001. Propagation of the thrust system and erosion in the Lesser Himalaya: Geochemical and sedimentological evidence. Geology 29(11), 1007–1010.

Huyghe, P., Mugnier, J.L., Gajurel, A.P., Delcaillau, B., 2005. Tectonic and climatic control of the changes in the sedimentary record of the Karnali River section (Siwaliks of western Nepal). Island Arc 14(4), 311–327.

Joussain, R., Colin, C., Liu, Z., Meynadier, L., Fournier, L., Fauquembergue, K., Zaragosi, S., Schmidt, F., Rojas, V., Bassinot, F., 2016. Climatic control of sediment transport from the Himalayas to the proximal NE Bengal Fan during the last glacial-interglacial cycle. Quaternary Sci. Rev. 148, 1–16.

Lang, K.A., Huntington, K.W., 2014. Antecedence of the Yarlung-Siang-Brahmaputra River, eastern Himalaya. Earth Planet. Sci. Lett. 397, 145–158.

Lang, K.A., Huntington, K.W., Burmester, R., Housen, B, 2016. Rapid exhumation of the eastern Himalayan syntaxis since the late Miocene. Geol. Soc. Am. Bull. 128(9), 1403–1422.

Licht, A., Reisberg, L., France-Lanord, C., Soe, A.N., Jaeger, J.J., 2016. Cenozoic evolution of the Central Myanmar drainage system: insights from sediment provenance in the Minbu Sub-Basin. Basin Res. 28(2), 237–251.

Licht, A., Dupont-Nivet, G., Win, Z., Swe, H.H., Kaythi, M., Roperch, P., Ugrai, T., Littell, V., Park, D., Westerweel, J., Jones, D., Poblete, F., Aung, D.W., Huang, H., Hoorn, C., Sein, K., 2018. Paleogene evolution of the Burmese forearc basin and implications for the history of India-Asia convergence. Geol. Soc. Am. Bull. 131 (5-6), 730–748. https://doi.org/10.1130/B35002.1.

Lin, T.H., Mitchell, A.H., Chung, S.L., Tan, X.B., Tang, J.T., Oo, T., Wu, F.Y., 2019. Two parallel magmatic belts with contrasting isotopic characteristics from southern Tibet to Myanmar: zircon U–Pb and Hf isotopic constraints. J. Geol. Soc. 176(3), 574–587.

McNeill, L.C., Dugan, B., Petronotis, K.E., the Expedition 362 Scientists, 2017a. Sumatra Subduction Zone. Proc. IODP, vol. 362. International Ocean Discovery Program, College Station, TX.

McNeill, L.C., Dugan, B., Backman, J., Pickering, K.T., Pouderoux, H.F.A., Henstock, T.J., Petronotis, K.E., Carter, A., Chemale Jr., F., Milliken, K.L., Kutterolf, S., Mukoyoshi, H., Chen, W., Kachovich, S., Mitchison, F.L., Bourlange, S., Colson, T.A., Frederik, M.C.G., Guèrin, G., Hamahashi, M., House, B.M., Hüpers, A., Jeppson, T.N., Kenigsberg, A.R., Kuranaga, M., Nair, N., Owari, S., Shan, Y., Song, I., Torres, M.E., Vannucchi, P., Vrolijk, P.J., Yang, T., Zhao, X., and Thomas, E., 2017b. Understanding Himalayan erosion and the significance of the Nicobar Fan. Earth Planet. Sci. Lett. 475, 134–142.

Najman, Y., Mark, C., Barfod, D. N., Carter, A., Parrish, R., Chew, D., Gemignani, L.

2019. Spatial and temporal trends in exhumation of the Eastern Himalaya and syntaxis as determined from a multitechnique detrital thermochronological study of the Bengal Fan. Geol. Soc. Am. Bull. 131 (9–10), 1607–1622. https://doi.org/10.1130/B35031.1

Pickering, K.T., Pouderoux, H., Carter, A., Andò, S., Garzanti, E., Limonta, M., Vezzoli, G., Milliken, K.L., Chemale Jr., F., Mukoyoshi, H., Kutterolf, S. 2018. Sediment Provenance and Depositional History of the Nicobar Fan (Bengal Depositional System) from IODP Expedition 362: Detrital Zircon Geochronology, Apatite Thermochronometry, Sand Petrography and Heavy-Mineral Results. In AGU Fall Meeting Abstracts.

Pickering, K.T., Pouderoux, H., McNeill, L.C., Backman, J., Chemale, F., Kutterolf, S., Milliken, K.L., Mukoyoshi, H., Henstock, Timothy, J., Stevens, D.E., Parnell, C., Dugan, B., 2020. Sedimentology, stratigraphy and architecture of the Nicobar Fan (Bengal–Nicobar Fan System), Indian Ocean: Results from International Ocean Discovery Program Expedition 362. Sedimentology. doi: 10.1111/sed.12701.

Racey, A., Ridd, M.F., 2015. Petroleum geology of the Moattama region, Myanmar, in: Racey, A., Ridd, M.F. (Eds.), Petroleum geology of Myanmar. Geol. Soc. Lond. Mem. 45, pp. 63–81.

Robinson, R.A.J., Brezina, C.A., Parrish, R.R., Horstwood, M.S.A., Oo, N.W., Bird, M.I., Thein, M., Walters, A.S., Oliver, G.J.H., Zaw, K., 2014. Large rivers and orogens: The evolution of the Yarlung Tsangpo-Irrawaddy system and the eastern Himalayan syntaxis. Gondwana Res. 26(1), 112–121.

Rudnick, R.L., Gao, S., 2003. Composition of the continental crust, in: Rudnick, R.L.

(Ed.), Treatise on Geochemistry, vol. 3, The Crust. Elsevier, New York, pp. 1–64.

Seward, D., Burg, J. P., 2008. Growth of the Namche Barwa Syntaxis and associated evolution of the Tsangpo Gorge: constraints from structural and thermochronological data. Tectonophysics 451, 282–289.

Singh, S.K., France-Lanord, C., 2002. Tracing the distribution of erosion in the Brahmaputra watershed from isotopic compositions of stream sediments. Earth Planet. Sci. Lett. 202(3), 645–662.

Singh, S.K., Rai, S.K., Krishnaswami, S., 2008. Sr and Nd isotopes in river sediments from the Ganga Basin: Sediment provenance and spatial variability in physical erosion. J. Geophys. Res. Earth Surface, 113: F03006.

Sun, S.S., McDonough, W.S., 1989. Chemical and isotopic systematics of oceanic basalts: Implications for mantle composition and processes. Geol. Soc. London, Spec. Publ. 42(1), 313–345. https://doi.org/10.1144/GSL.SP.1989.042.01.19

Szulc, A.G., Najman, Y., Sinclair, H.D., Pringle, M., Bickle, M., Chapman, H., Garzanti E., Andò, DeCelles, P., 2006. Tectonic evolution of the Himalaya constrained by detrital ^{40}Ar-^{39}Ar, Sm-Nd and petrographic data from the Siwalik foreland basin succession, SW Nepal. Basin Res. 18(4), 375–391.

Wu, W., Xu, S., Yang, J., Yin, H., Lu, H., Zhang, K., 2010. Isotopic characteristics of river sediments on the Tibetan Plateau. Chem. Geol. 269(3–4), 406–413.

Yin, A., 2006. Cenozoic tectonic evolution of the Himalayan orogen as constrained by along-strike variation of structural geometry, exhumation history, and foreland sedimentation. Earth-Sci. Rev. 76(1–2), 1–131.

Zeitler, P.K., Meltzer, A.S., Koons, P.O., Craw, D., Hallet, B., Chamberlain, C.P., Kidd, W.S.F., Park, S.K., Seeber, L., Bishop, M., Shroder, J., 2001. Erosion, Himalayan geodynamics, and the geomorphology of metamorphism. GSA Today 11: 4–8.

Zeitler, P.K., Meltzer, A.S., Brown, L., Kidd, W.S.F., Lim, C., Enkelmann, E., 2014. Tectonics and topographic evolution of Namche Barwa and the easternmost Lhasa Block, in: Nie, J., Hoke, G.D., Horton, B. (Eds.), Towards an Improved Understanding of Uplift Mechanisms and the Elevation History of the Tibetan Plateau. Spec. Pap., Geol. Soc. of Am. 507, 23–58.

Figure Captions (color online only for all figures)

Fig. 1. Regional map of the Bengal-Nicobar Fan system, showing the IODP Expedition 362 sites (U1480 and U1481) on the Nicobar Fan and the relevant drilling sites of DSDP Leg 22 (Site 218), ODP Leg 116 (Sites 717 and 718) and IODP Expedition 354 (Sites U1449–U1455). The superimposed simplified geological map of the eastern Himalaya, southeastern Tibet and Myanmar region, showing major terrains, terrain boundaries, geological units and modern major rivers, is modified from Robinson et al. (2014) and Licht et al. (2016). The Bengal Fan and the Nicobar Fan are outlined in black and grey, respectively (after Pickering et al., 2020). The Martaban basin in the eastern Andaman Sea is delineated by 3 km isopach (Racey and Ridd, 2015) in purple.

Fig. 2. Schematic lithological columns of Sites U1480 and U1481 modified from McNeill et al. (2017a), showing the position of the Nicobar Fan samples.

Fig. 3. (a) Upper continental crust (UCC) (Rudnick and Gao, 2003) normalized for trace

elements in the Nicobar Fan samples, as compared with the Neogene sediments of the Surma Basin (Hossain et al., 2010) and the Bengal Fan (Crowley et al., 1998). (b) Chondrite-normalized REE distribution plot for the Nicobar Fan samples as compared with the UCC and the Neogene sediments of the Surma Basin (Hossain et al., 2010) and the Bengal Fan (Crowley et al., 1998). The chondrite values are cited from Sun and McDonough (1989).

Fig. 4. Downhole variation of Th, Ta and Nb concentrations, and Cr/Th, La/Lu and La_N/Yb_N ratios of the Nicobar Fan sediments at both Sites U1480 and U1481. Age of the Site U1480 and U1481 samples is converted from the mid-point depth according to age models of Backman et al. (2019) and McNeil et al (2017a), respectively.

Fig. 5. Downhole variation of Sr-Nd isotopic compositions of the Nicobar Fan sediments at both Sites U1480 and U1481, as compared with the Sr-Nd isotopic compositions of contemporary sediments in the Bengal Fan (France-Lanord et al., 1993; Galy et al., 1996; Galy et al., 2010), the Surma Basin (Bracciali et al., 2015), the eastern Himalayan foreland (Chirouze et al., 2013) and the Nepalese foreland (Huyghe et al., 2001, 2005; Szulc et al., 2006) and modern sediments in the Brahmaputra and the Ganges mainstreams (Singh and France-Lanord, 2002; Singh et al., 2008). All the ε_{Nd} values and $^{87}Sr/^{86}Sr$ ratios are recalculated at time T=0, and depositional ages of the Surma Basin samples are of large uncertainties. Also shown are the sedimentation rate of Sites U1480 and U1481 (McNeill et al., 2017a, Backman et al., 2019), ODP Site 718C (after McNeill et al., 2017b) and DSDP Site 218 (Galy et al., 2010), the proportion of detrital zircons

<150 Ma of the Nicobar Fan samples (McNeill et al. 2017b), and the associated Himalayan tectonic events. GR=Ganges River, BR=Brahmaputra River, NER=Ninetyeast Ridge.

Fig. 6. ε_{Nd} vs Th, Ta, Nb contents and Cr/Th, La/Lu and La_N/Yb_N ratios for the Niocbar Fan samples. The grey dash lines in the plots represent the regression lines.

Fig. 7. (a) ε_{Nd} vs $^{87}Sr/^{86}Sr$ plot of the Nicobar Fan samples, as compared with the potential source rocks from the Himalaya-Tibet region and the modern sediments in the Brahmaputra and the Ganges mainstreams (see Table1 for references). The composition fields of the Neogene sediments in the Bengal Fan, the Surma Basin and the Nepalese foreland are also shown (France-Lanord et al., 1993; Galy et al., 1996; Galy et al., 2000; Bracciali et al., 2015; Huyghe et al., 2001; 2005). (b) A simple two-components mixing model based on Sr-Nd isotopes for the Nicobar Fan sediments. End-member compositions used in the model are: the Greater Himalaya: Sr=70 ppm, Nd=45 ppm, $^{87}Sr/^{86}Sr$=0.760, ε_{Nd}=-16 (Singh and France-Lanord, 2002; Singh et al., 2008); the Gangdese arc: Sr=200 ppm, Nd=34 ppm; $^{87}Sr/^{86}Sr$=0.715; ε_{Nd}=-6.8 (Wu et al., 2010). The latter is based on the average of the modem river sediments from the tributaries and mainstream of the Yarlung Tsangpo that drain the southern Lhasa block. It should be noted that in this calculation the proportion of the Gangdese arc also includes the Pre-Cambrian basement rocks (the Nyainqêntanglha Group) and the Paleozoic–Mesozoic sedimentary cover of the Lhasa block and even the Northern Magmatic belt intruded the northern Lhasa block, besides the Cretaceous–Paleogene magmatic and volcanic rocks

(the Gangdese batholith and Linzizong volcanics) in the southern Lhasa block, because the tributaries of the Yarlung Tsangpo also drain these units. This might be one of the reasons why the proportion of Gangdese arc material derived from this model is much higher than the proportion of typical Gangdese zircons (<150 Ma) in the Nicobar Fan sand/sandstone (McNeil et al., 2017b) in Fig. 5 (other reasons might include the abundance of zircons in parent rocks and hydraulic sorting of detrital zircons during transport).

Fig. 8. Paleogeography reconstruction of the region of the northeastern Indian Ocean (adapted from Hall, 2012), showing drainage evolution of the Ganges River and the Yarlung Tsangpo-Brahmaputra River (modified from Lang and Huntington, 2014; Govin et al., 2018) and the source-to-sink process from the Himalaya to the Bengal-Nicobar Fan system. GR=Ganges River, BR=Brahmaputra River, IR=Irrawaddy River, SP=Shillong Plateau, IBR=Indo-Burman Ranges, WPA=Wuntho-Popa Arc (Burmese arc), NER=Ninetyeast Ridge.

Tables

Table 1. $^{87}Sr/^{86}Sr$ ratios and ε_{Nd} values of geologic units and major rivers of the Himalaya, Tibet and Myanmar domain

Potential Source	$^{87}Sr/^{86}Sr$	ε_{Nd}	References
	Himalaya and Tibet domain		
Lesser Himalaya	0.72–0.94	-25.3 to -23.5	Singh et al. (2008) and references therein
Greater Himalaya	0.73–0.79	-18 to -13.6	Singh and France-Lanord (2002); Singh et al. (2008) and references therein
Tethyan Himalaya	0.71–0.73	-15 to -12	Singh et al. (2008) and references therein
Gangdese arc (volcanics and granitoids in the southern Lhasa block)	0.70–0.73	-9 to +6	Wu et al. (2010) and references therein
	Myanmar domain		

Paleogene Indo-Burman Ranges	0.714–0.716	-8.6 to -4.0	Colin et al. (1999); Allen et al. (2008)
Burmese arc (Wuntho-Popa Arc and intrusive rocks in Mogok Metamorphic Belt)	0.70–0.73	-10 to +4	Lin et al. (2019)
	Major Rivers		
Ganges River (mainstream)	0.748–0.787	-21.3 to -15.7	Singh et al. (2008)
Brahmaputra River (mainstream)	0.718–0.749	-16.9 to -12.5	Singh and France-Lanord (2002)
Irrawaddy River	0.713–0.714	-8.3 to -10.7	Colin et al. (1999); Allen et al. (2008)

[*]All the ε_{Nd} values and $^{87}Sr/^{86}Sr$ ratios are recalculated at time T=0.

Appendix A. Supplementary materials

Full Analytical Method

Table A.1. Trace elements of the Nicobar Fan sediments

Table A.2. Sr-Nd isotope composition of the Nicobar Fan sediments

Fig. A.1. Cr/Th versus Th/Sc diagram for the Nicobar Fan sediments

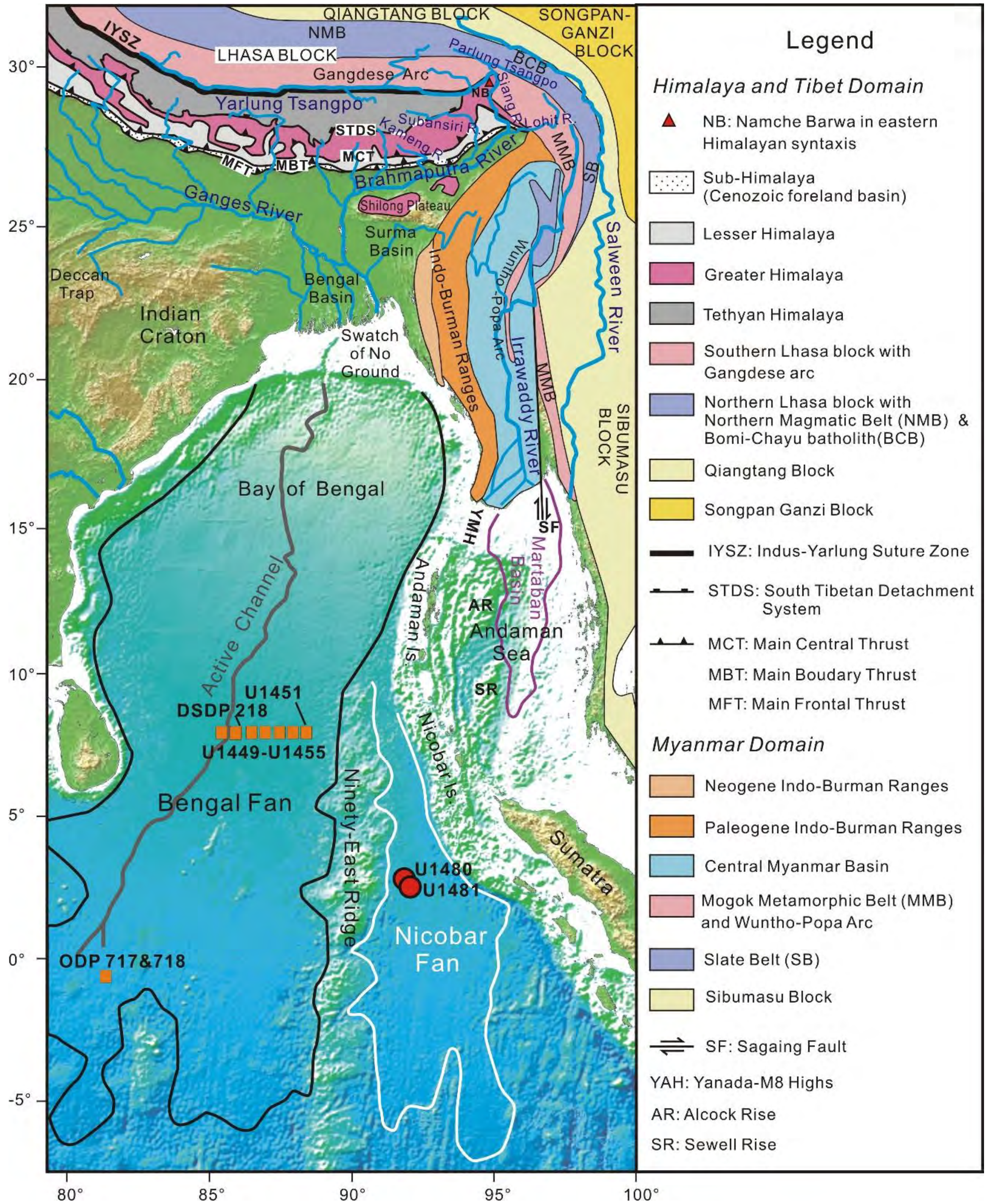
QIANGTANG BLOCK
SONGPAN-GANZI BLOCK
NMB
IYSZ
LHASA BLOCK
Gangdese Arc
Parlung Tsangpo
BCB
NB
Siang R.
Lohit R.
Yarlung Tsangpo
Subansiri R.
Kameng R.
STDS
MCT
MFT
MBT
Brahmaputra River
MMB
SB
Ganges River
Shilong Plateau
Surma Basin
Salween River
Deccan Trap
Indian Craton
Bengal Basin
Indo-Burman Ranges
Wuntho-Popa Arc
Irrawaddy River
Swatch of No Ground
SIBUMASU BLOCK
Bay of Bengal
YMH
SF
Martaban Basin
Active Channel
Andaman Is
AR
Andaman Sea
SR
U1451
DSDP 218
U1449-U1455
Nicobar Is
Bengal Fan
Ninety-East Ridge
Sumatra
U1480
U1481
Nicobar Fan
ODP 717&718
30°
25°
20°
15°
10°
5°
0°
-5°
80°
85°
90°
95°
100°
Legend
Himalaya and Tibet Domain
NB: Namche Barwa in eastern Himalayan syntaxis
Sub-Himalaya (Cenozoic foreland basin)
Lesser Himalaya
Greater Himalaya
Tethyan Himalaya
Southern Lhasa block with Gangdese arc
Northern Lhasa block with Northern Magmatic Belt (NMB) & Bomi-Chayu batholith(BCB)
Qiangtang Block
Songpan Ganzi Block
IYSZ: Indus-Yarlung Suture Zone
STDS: South Tibetan Detachment System
MCT: Main Central Thrust
MBT: Main Boudary Thrust
MFT: Main Frontal Thrust
Myanmar Domain
Neogene Indo-Burman Ranges
Paleogene Indo-Burman Ranges
Central Myanmar Basin
Mogok Metamorphic Belt (MMB) and Wuntho-Popa Arc
Slate Belt (SB)
Sibumasu Block
SF: Sagaing Fault
YAH: Yanada-M8 Highs
AR: Alcock Rise
SR: Sewell Rise

Fig. 1

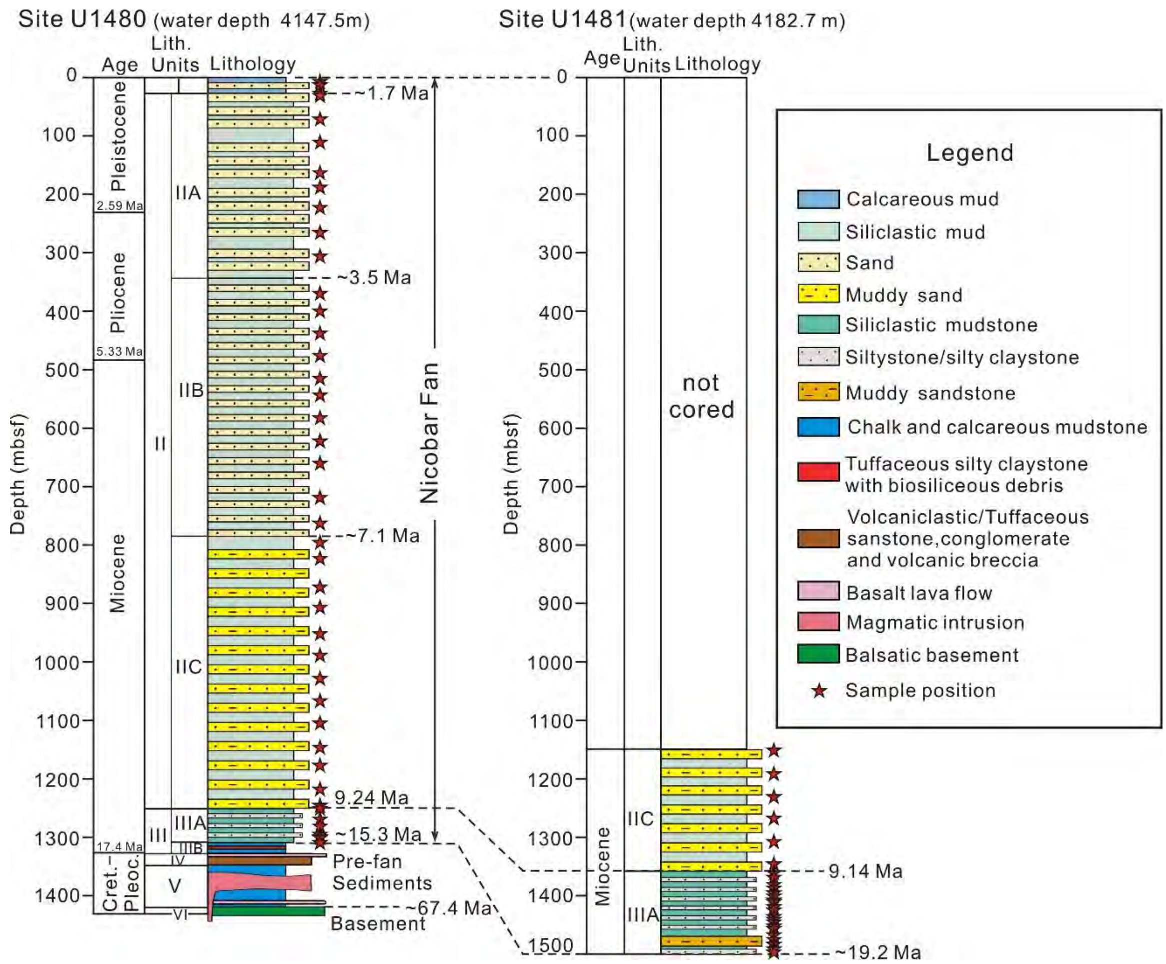
Site U1480 (water depth 4147.5m)
Age
Lith. Units
Lithology
Depth (mbsf)
0
100
200
300
400
500
600
700
800
900
1000
1100
1200
1300
1400
Pleistocene
2.59 Ma
Pliocene
5.33 Ma
Miocene
17.4 Ma
Cret.-Pleoc.
IIA
IIB
II
IIC
IIIA
III
IIIB
IV
V
VI
~1.7 Ma
~3.5 Ma
~7.1 Ma
9.24 Ma
~15.3 Ma
~67.4 Ma
Nicobar Fan
Pre-fan Sediments
Basement
Site U1481 (water depth 4182.7 m)
Age
Lith. Units
Lithology
Depth (mbsf)
not cored
Miocene
IIC
IIIA
9.14 Ma
~19.2 Ma
1500
Legend
Calcareous mud
Siliclastic mud
Sand
Muddy sand
Siliclastic mudstone
Siltystone/silty claystone
Muddy sandstone
Chalk and calcareous mudstone
Tuffaceous silty claystone with biosiliceous debris
Volcaniclastic/Tuffaceous sanstone, conglomerate and volcanic breccia
Basalt lava flow
Magmatic intrusion
Balsatic basement
Sample position

Fig. 2

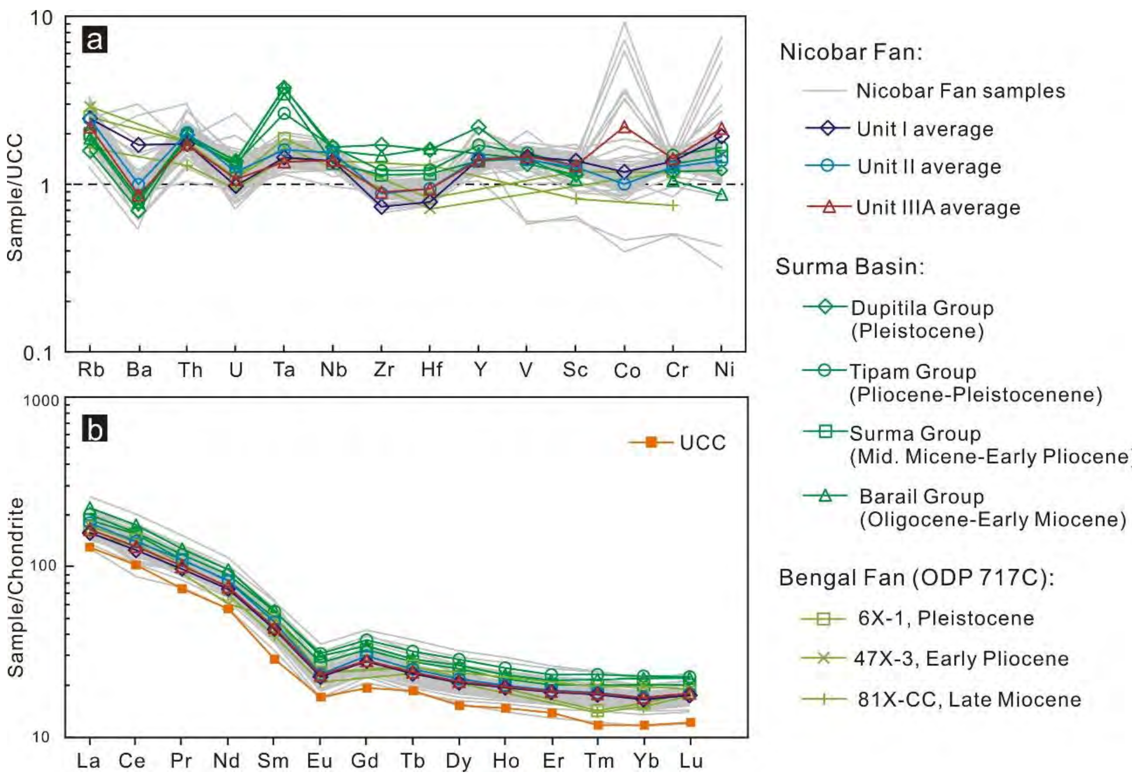
a
Sample/UCC
10
1
0.1
Rb
Ba
Th
U
Ta
Nb
Zr
Hf
Y
V
Sc
Co
Cr
Ni
b
Sample/Chondrite
1000
100
10
UCC
La
Ce
Pr
Nd
Sm
Eu
Gd
Tb
Dy
Ho
Er
Tm
Yb
Lu
Nicobar Fan:
Nicobar Fan samples
Unit I average
Unit II average
Unit IIIA average
Surma Basin:
Dupitila Group (Pleistocene)
Tipam Group (Pliocene-Pleistocenene)
Surma Group (Mid. Micene-Early Pliocene)
Barail Group (Oligocene-Early Miocene)
Bengal Fan (ODP 717C):
6X-1, Pleistocene
47X-3, Early Pliocene
81X-CC, Late Miocene

Fig. 3

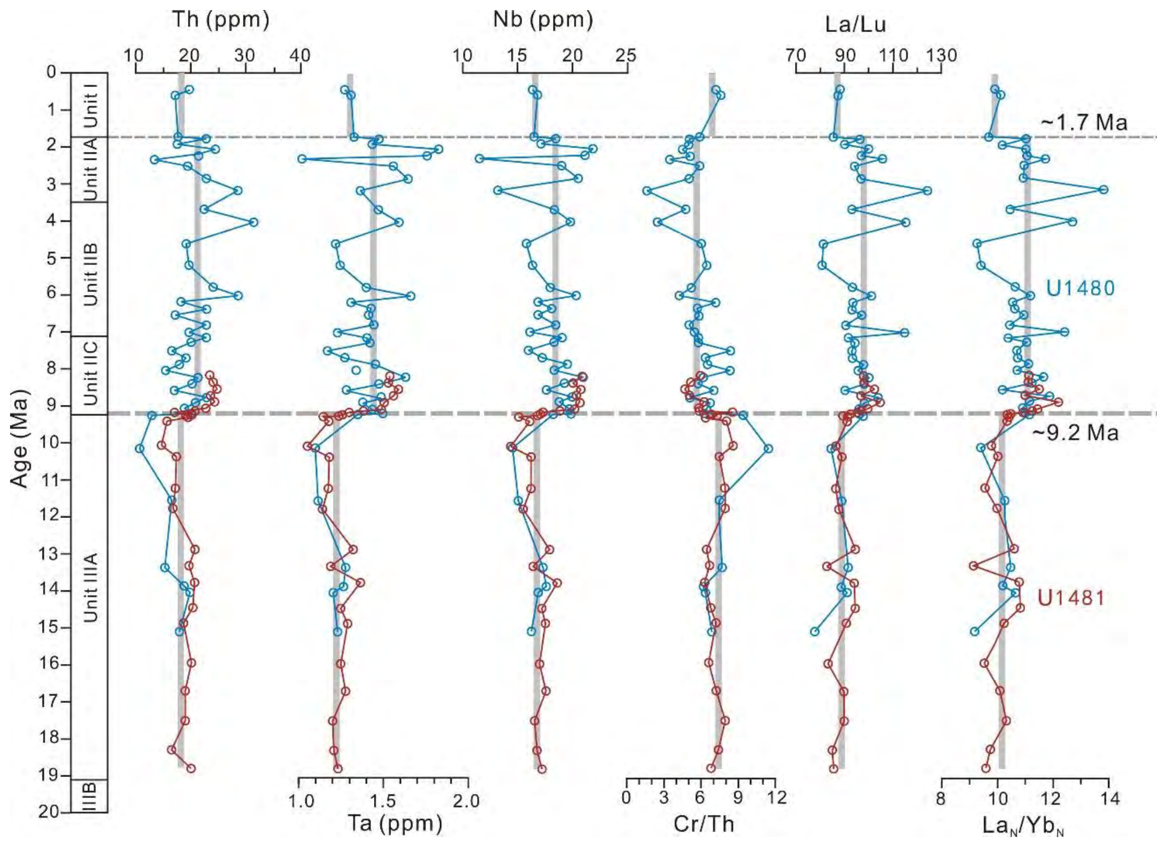
Th (ppm)
10 20 30 40
Nb (ppm)
10 15 20 25
La/Lu
70 90 110 130
Age (Ma)
Unit I
Unit IIA
Unit IIB
Unit IIC
Unit IIIA
IIIB
~1.7 Ma
~9.2 Ma
U1480
U1481
1.0 1.5 2.0
Ta (ppm)
0 3 6 9 12
Cr/Th
8 10 12 14
La_N/Yb_N

Fig. 4

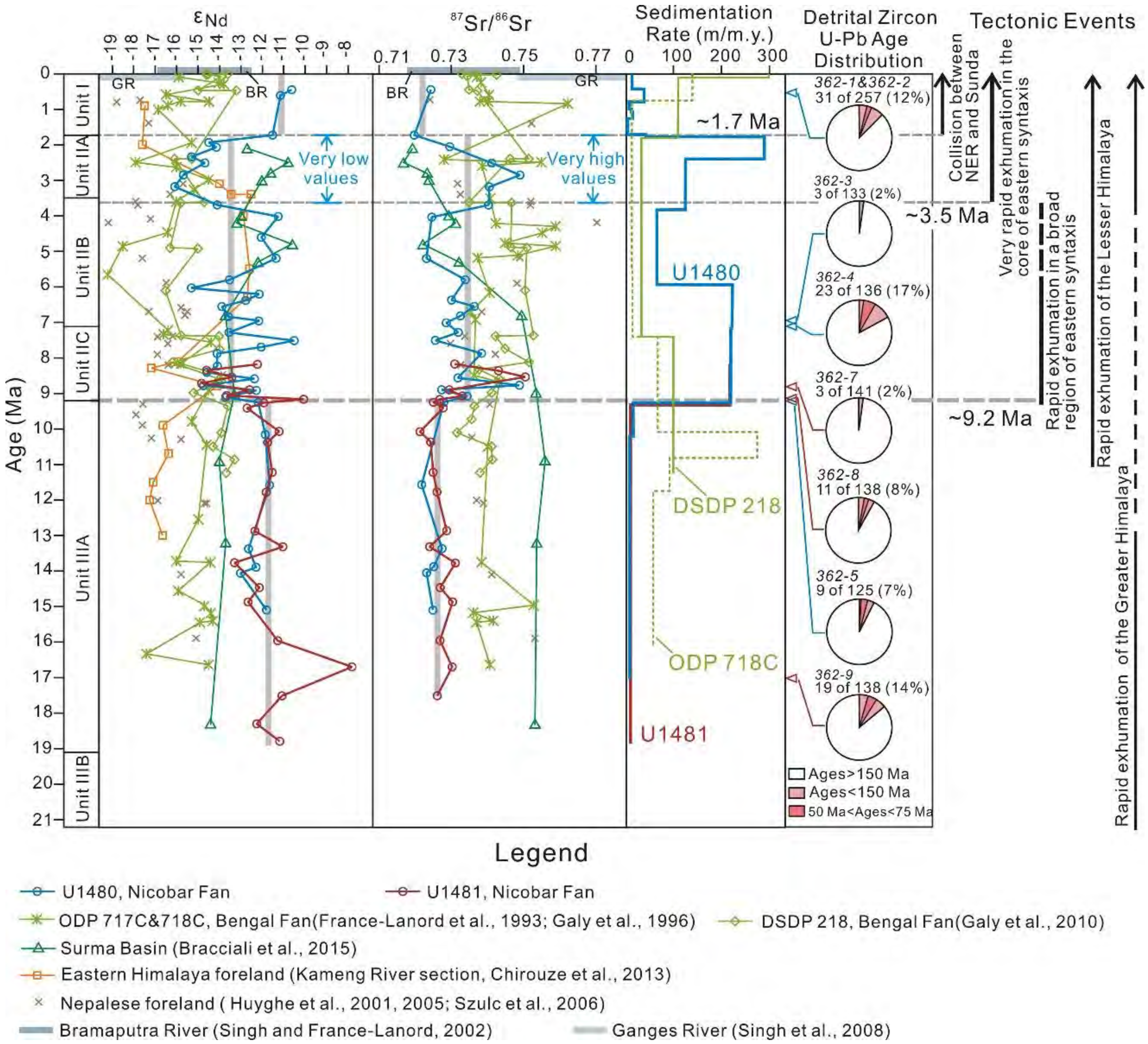
εNd
87Sr/86Sr
Sedimentation Rate (m/m.y.)
Detrital Zircon U-Pb Age Distribution
Tectonic Events
Age (Ma)
Unit I
Unit IIA
Unit IIB
Unit IIC
Unit IIIA
Unit IIIB
GR
BR
Very low values
Very high values
~1.7 Ma
~3.5 Ma
~9.2 Ma
U1480
U1481
DSDP 218
ODP 718C
362-1&362-2
31 of 257 (12%)
362-3
3 of 133 (2%)
362-4
23 of 136 (17%)
362-7
3 of 141 (2%)
362-8
11 of 138 (8%)
362-5
9 of 125 (7%)
362-9
19 of 138 (14%)
Ages>150 Ma
Ages<150 Ma
50 Ma<Ages<75 Ma
Collision between NER and Sunda
Very rapid exhumation in the core of eastern syntaxis
Rapid exhumation in a broad region of eastern syntaxis
Rapid exhumation of the Lesser Himalaya
Rapid exhumation of the Greater Himalaya
Legend
U1480, Nicobar Fan
U1481, Nicobar Fan
ODP 717C&718C, Bengal Fan(France-Lanord et al., 1993; Galy et al., 1996)
DSDP 218, Bengal Fan(Galy et al., 2010)
Surma Basin (Bracciali et al., 2015)
Eastern Himalaya foreland (Kameng River section, Chirouze et al., 2013)
Nepalese foreland (Huyghe et al., 2001, 2005; Szulc et al., 2006)
Bramaputra River (Singh and France-Lanord, 2002)
Ganges River (Singh et al., 2008)

Fig. 5

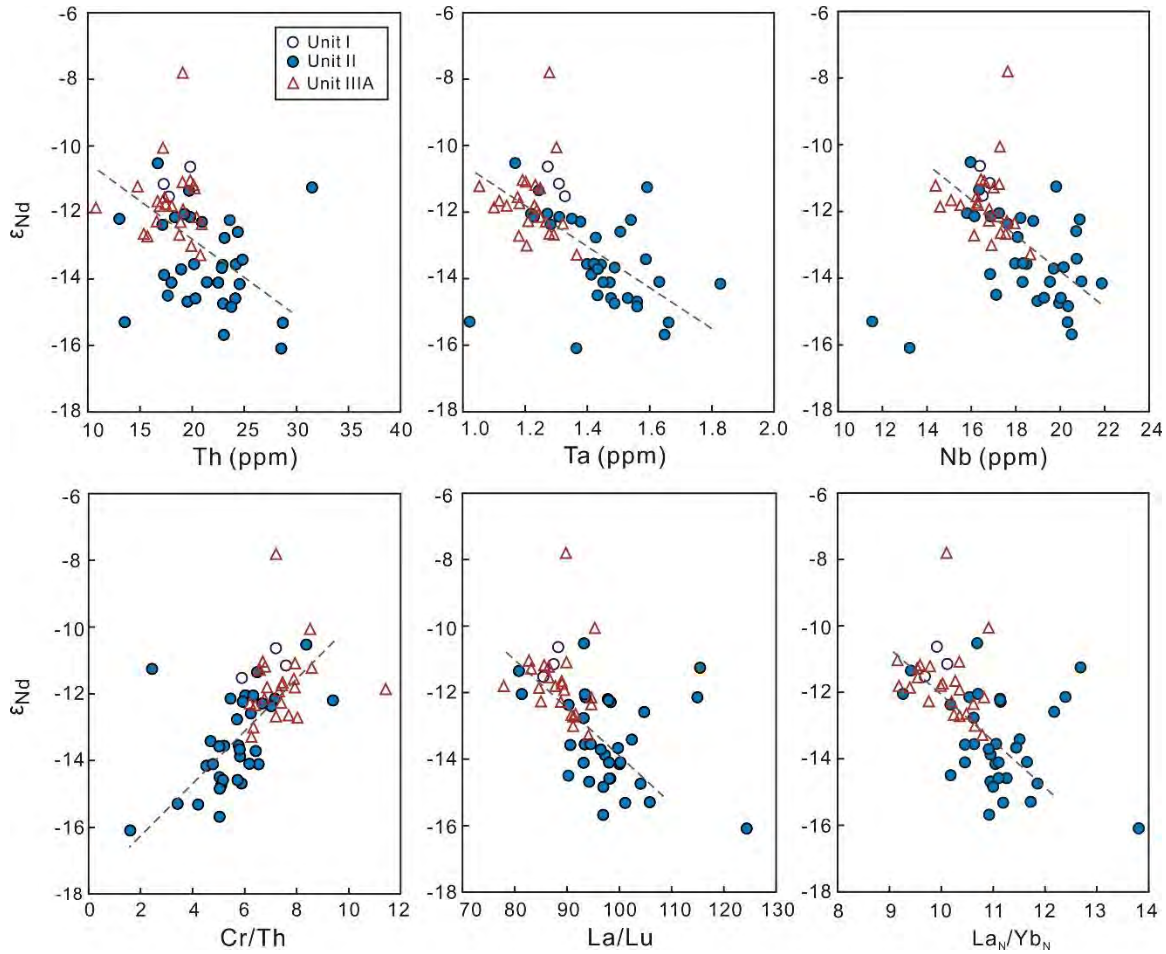

Unit I
Unit II
Unit IIIA
εNd
Th (ppm)
Ta (ppm)
Nb (ppm)
Cr/Th
La/Lu
La_N/Yb_N

Fig. 6

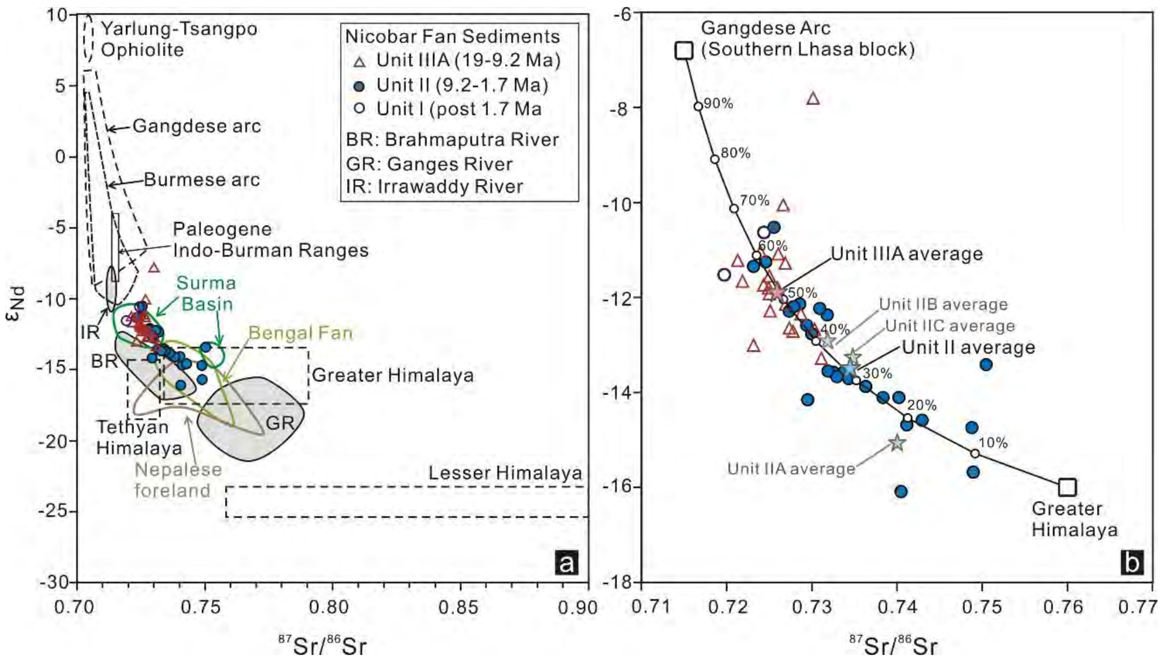
Yarlung-Tsangpo
Ophiolite
Gangdese arc
Burmese arc
Paleogene
Indo-Burman Ranges
Surma
Basin
Bengal Fan
Greater Himalaya
Tethyan
Himalaya
Nepalese
foreland
Lesser Himalaya
IR
BR
GR
Nicobar Fan Sediments
Unit IIIA (19-9.2 Ma)
Unit II (9.2-1.7 Ma)
Unit I (post 1.7 Ma
BR: Brahmaputra River
GR: Ganges River
IR: Irrawaddy River
εNd
87Sr/86Sr
a
Gangdese Arc
(Southern Lhasa block)
90%
80%
70%
60%
50%
40%
30%
20%
10%
Unit IIIA average
Unit IIB average
Unit IIC average
Unit II average
Unit IIA average
Greater
Himalaya
b

Fig. 7

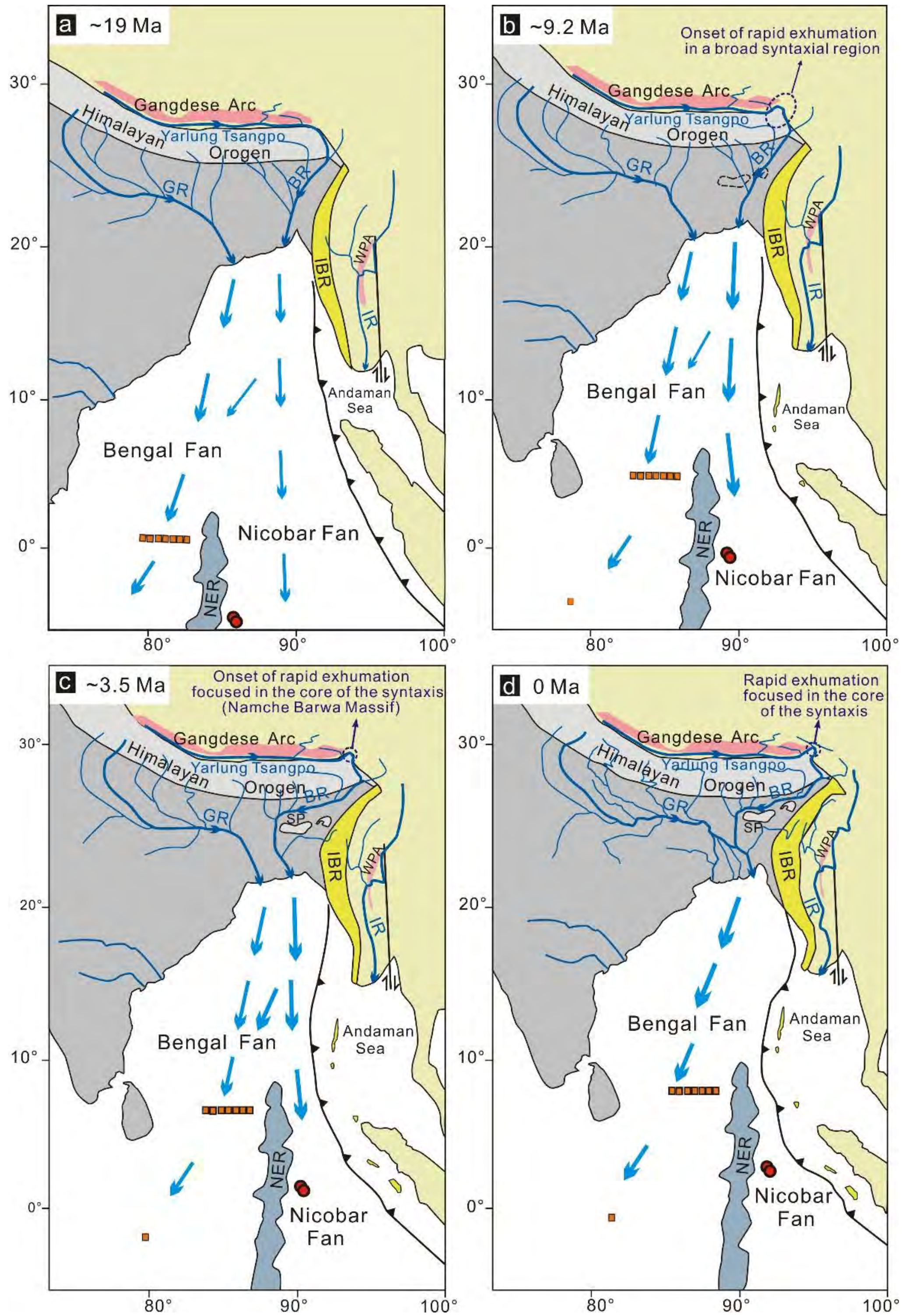

a ~19 Ma
30°
20°
10°
0°
80°
90°
100°
Gangdese Arc
Himalayan
Yarlung Tsangpo
Orogen
GR
BR
IBR
WPA
IR
Andaman Sea
Bengal Fan
Nicobar Fan
NER
b ~9.2 Ma
Onset of rapid exhumation in a broad syntaxial region
Gangdese Arc
Himalayan
Yarlung Tsangpo
Orogen
GR
BR
IBR
WPA
IR
Bengal Fan
Andaman Sea
NER
Nicobar Fan
c ~3.5 Ma
Onset of rapid exhumation focused in the core of the syntaxis (Namche Barwa Massif)
Gangdese Arc
Himalayan
Yarlung Tsangpo
Orogen
GR
BR
SP
IBR
WPA
IR
Bengal Fan
Andaman Sea
NER
Nicobar Fan
d 0 Ma
Rapid exhumation focused in the core of the syntaxis
Gangdese Arc
Himalayan
Yarlung Tsangpo
Orogen
GR
BR
SP
IBR
WPA
IR
Bengal Fan
Andaman Sea
NER
Nicobar Fan

Fig. 8

Figure 1

Click here to download Figure: Figure 1.pdf

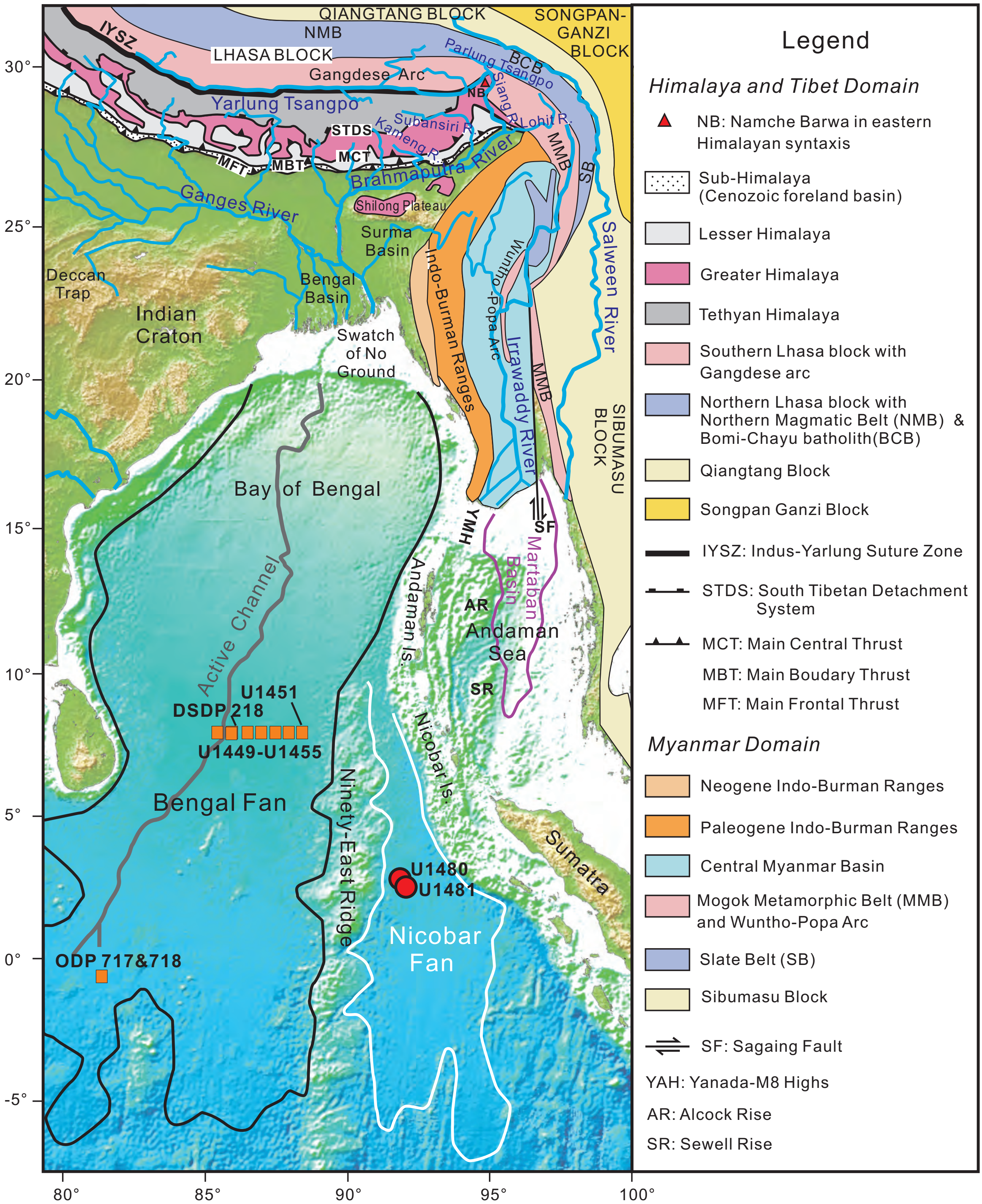

Figure 2

Click here to download Figure: Figure 2.pdf

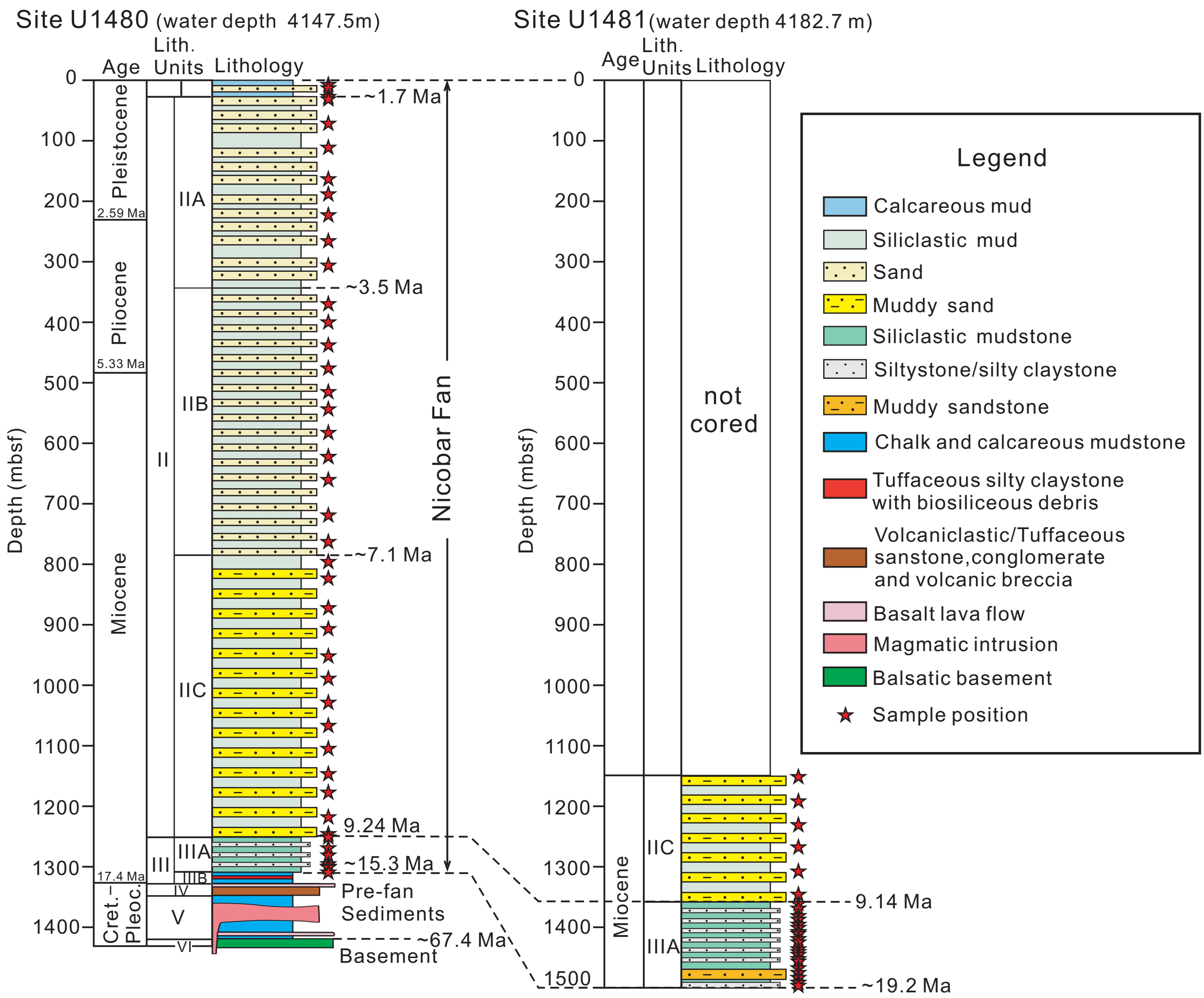

Figure 3

Click here to download Figure: Figure 3.pdf

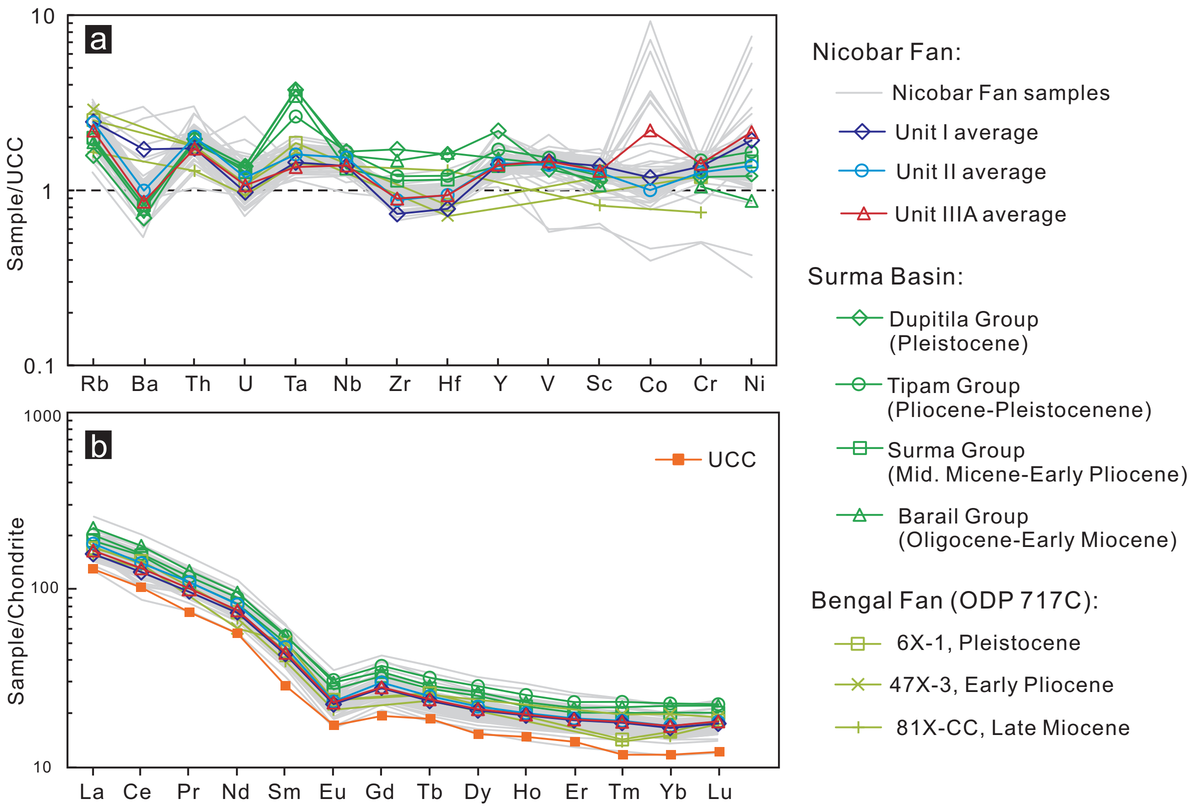

Figure 4
Click here to download Figure: Figure 4.pdf

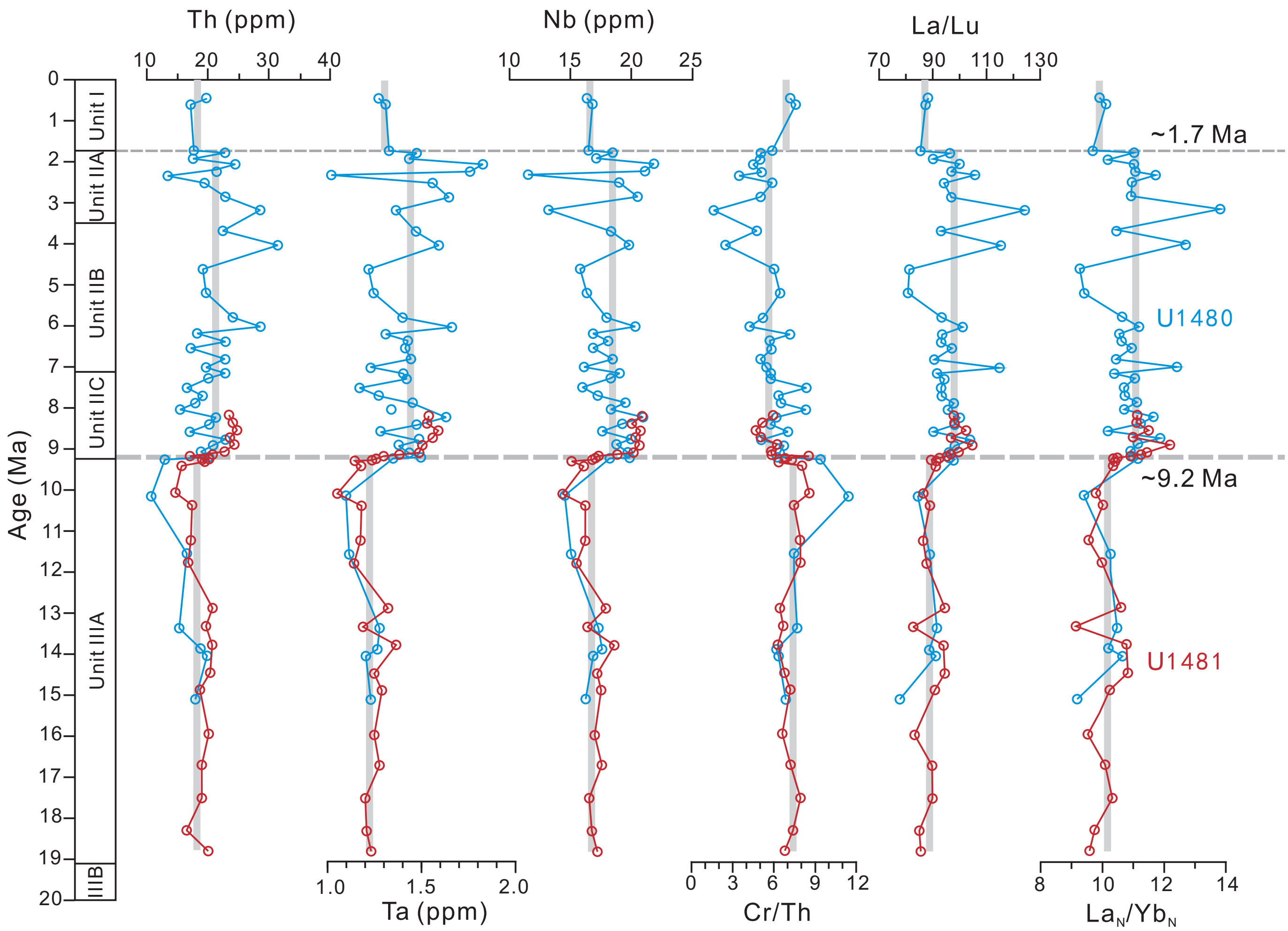

Figure 5

Click here to download Figure: Figure 5.pdf

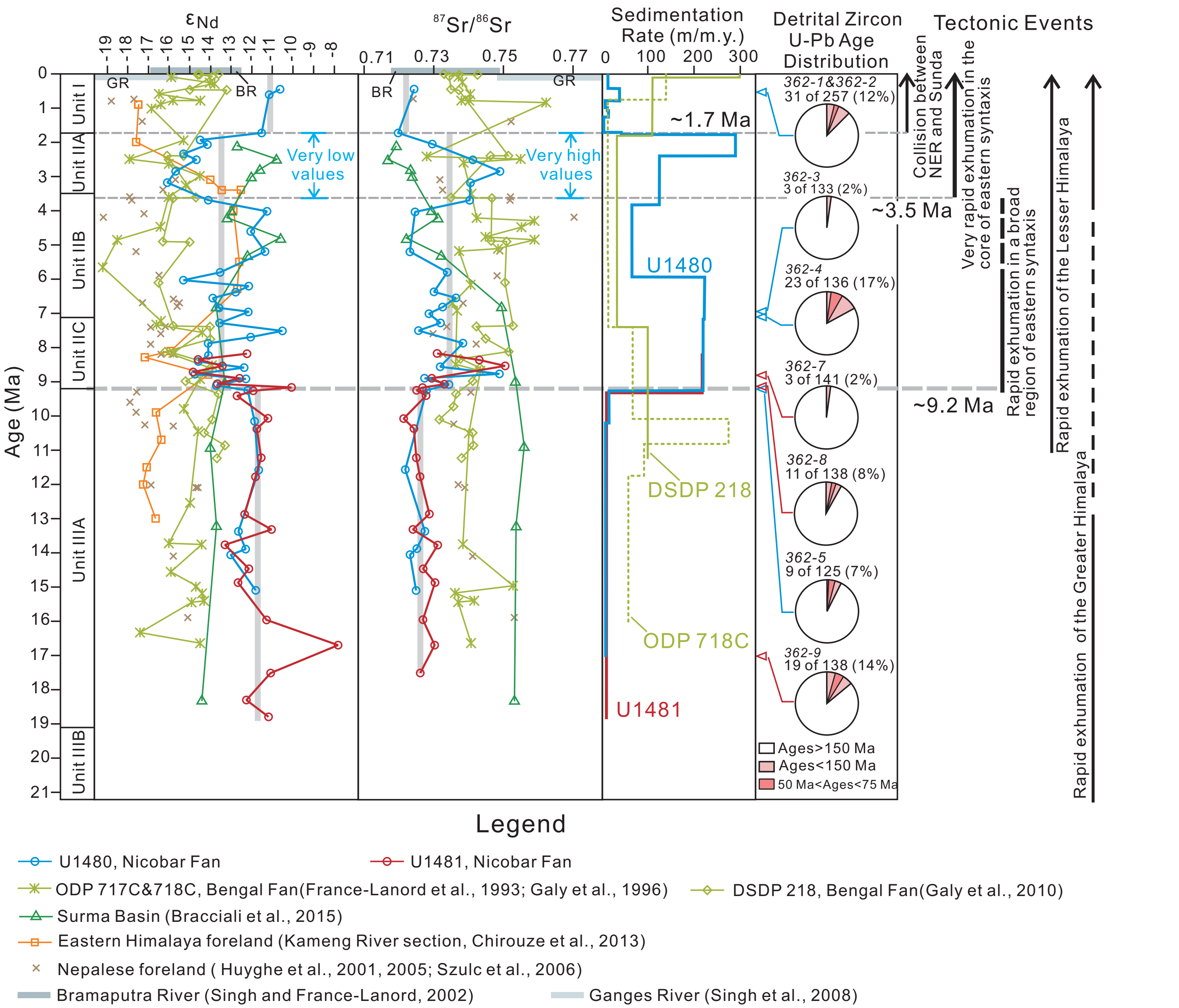

Figure 6
Click here to download Figure: Figure 6.pdf

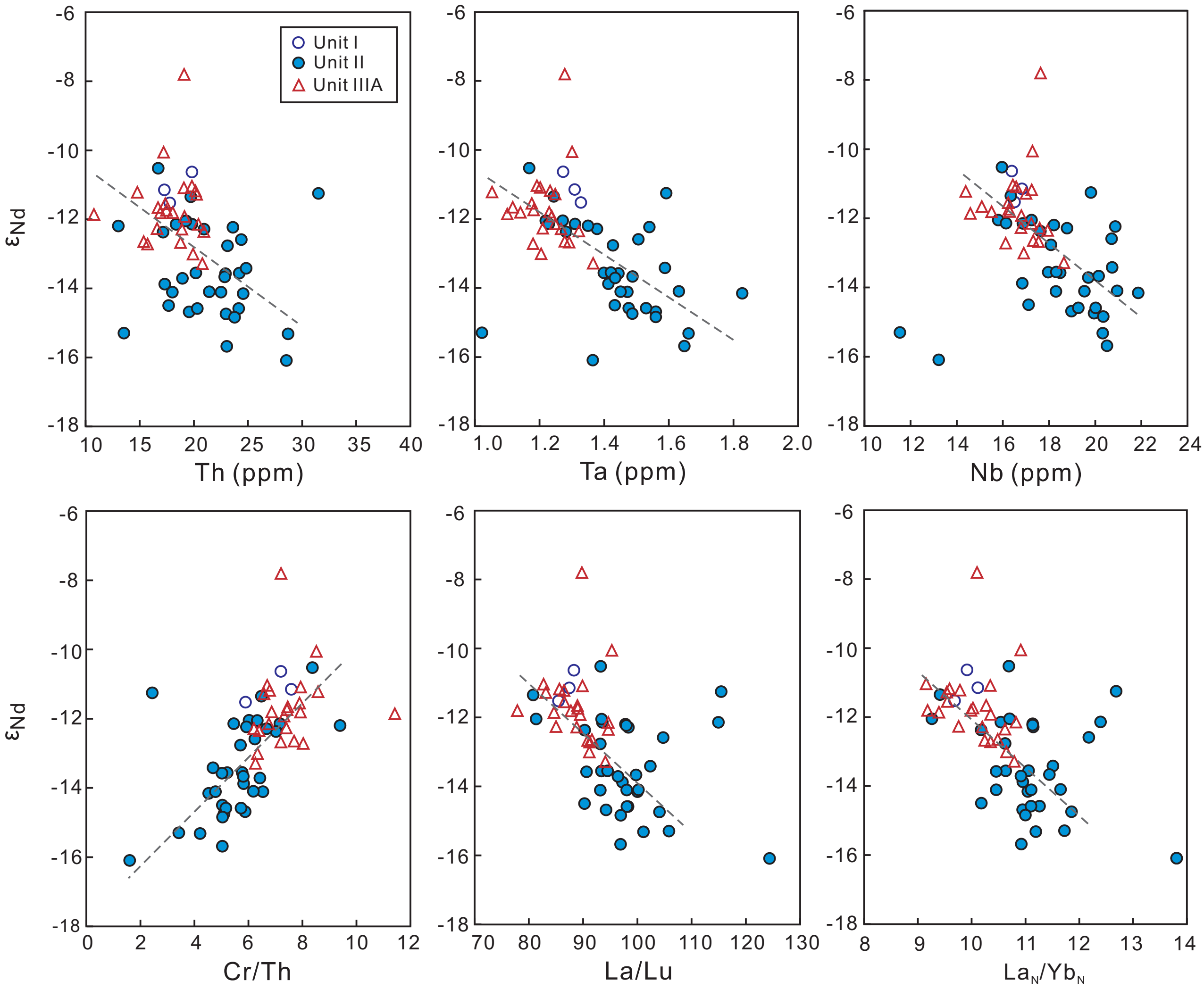

Figure 7
Click here to download Figure: Figure 7.pdf

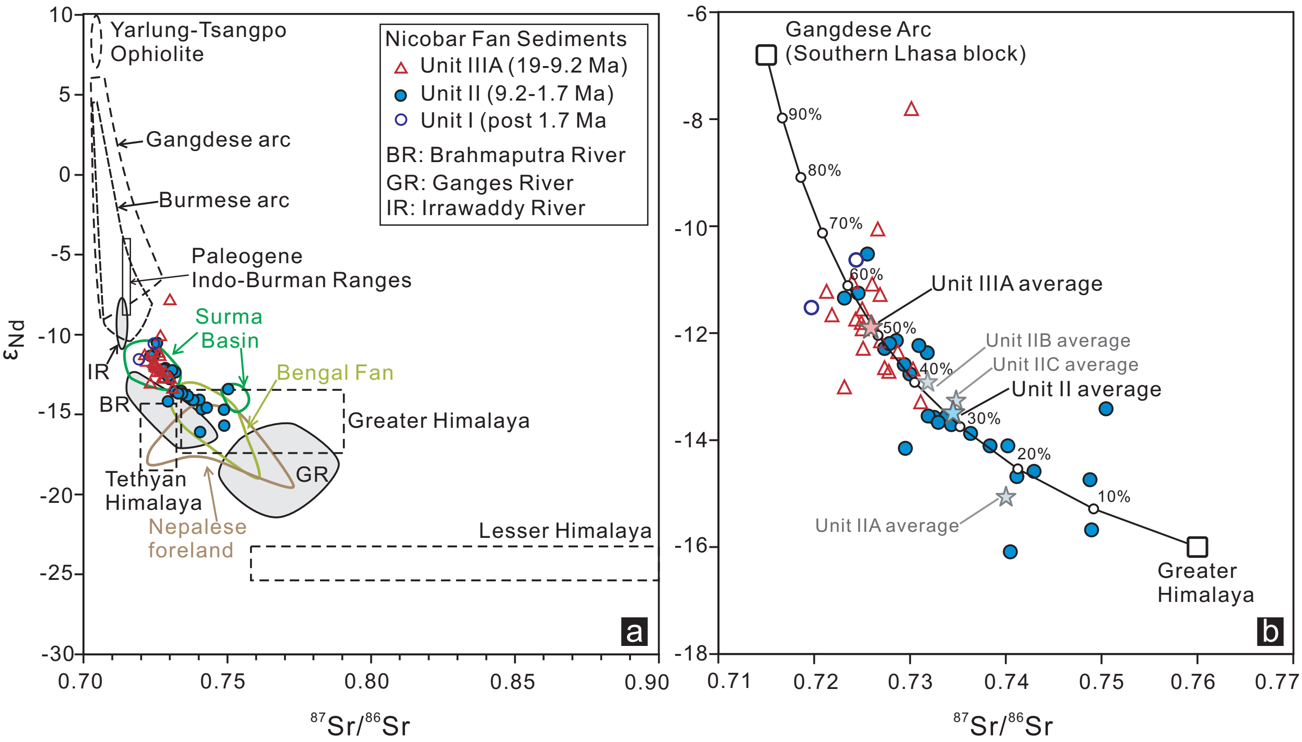

Figure 8

Click here to download Figure: Figure 8.pdf